Sub-seasonal behaviour of Asian summer monsoon under a changing climate: assessments using CMIP5 models

K. P. Sooraj, Pascal Terray, Prince K. Xavier

Sub-seasonal behaviour of Asian summer monsoon under a changing climate: assessments using CMIP5 models

Sooraj K P[1], Pascal Terray[1,2,3] and Prince K Xavier[4]

[1]Centre for Climate Change Research, Indian Institute of Tropical Meteorology, Pune 411008, India

[2]Sorbonne Universites (UPMC, Univ Paris 06)-CNRS-IRD-MNHN, LOCEAN Laboratory, 4 place Jussieu, Paris, France

[3]Indo-French cell for Water Sciences, IISc-IITM-NIO–IRD Joint International Laboratory, IITM, Pune 411008, India

[4]Met Office Hadley Centre, FitzRoy Road, Exeter, EX1 3PB, United Kingdom

Climate Dynamics (revised)

Jul, 2015

Corresponding author address:

Sooraj K. P.

Centre for Climate Change Research

Indian Institute of Tropical Meteorology

Pune 411008, India

e-mail: sooraj@tropmet.res.in

Abstract

Numerous global warming studies show the anticipated increase in mean precipitation with the rising levels of carbon dioxide concentration. However, apart from the changes in mean precipitation, the finer details of daily precipitation distribution, such as its intensity and frequency (so called daily rainfall extremes), need to be accounted for while determining the impacts of climate changes in future precipitation regimes. Here we examine the climate model projections from a large set of Coupled Model Inter-comparison Project 5 (CMIP5) models, to assess these future aspects of rainfall distribution over Asian Summer Monsoon (ASM) region. Our assessment unravels a north-south rainfall dipole pattern, with increased rainfall over Indian subcontinent extending into the western Pacific region (north ASM region, NASM) and decreased rainfall over equatorial oceanic convergence zone over eastern Indian Ocean region (south ASM region, SASM). This robust future pattern is well conspicuous at both seasonal and sub-seasonal time scales. Subsequent analysis, using daily rainfall events defined using percentile thresholds, demonstrates that mean rainfall changes over NASM region are mainly associated with more intense and more frequent extreme rainfall events (i.e. above 95^{th} percentile). The inference is that there are significant future changes in rainfall probability distributions and not only a uniform shift in the mean rainfall over the NASM region. Rainfall suppression over SASM seems to be associated with changes involving multiple rainfall events and shows a larger model spread, thus making its interpretation more complex compared to NASM. Moisture budget diagnostics generally show that the low-level moisture convergence, due to stronger increase of water vapour in the atmosphere, acts positively to future rainfall changes, especially for heaviest rainfall events. However, it seems that the dynamic component of moisture convergence, associated with vertical motion, shows a strong spatial and rainfall category dependency, sometimes offsetting the effect of the water vapour increase. Additionally, we found that the moisture

convergence is mainly dominated by the climatological vertical motion acting on the humidity changes and the interplay between all these processes proves to play a pivotal role for regulating the intensities of various rainfall events in the two domains.

Kew words:

Asian summer monsoon; precipitation characteristics; north-south rainfall dipole pattern; moist mechanisms; daily rainfall extremes

1. Introduction

Global climate change is no more a scientific curiosity now, as convincing evidences can be found in many facets of the climate system such as temperature increase, snow cover decrease, ice extent and thickness, sea level rise and more frequent extreme events (IPCC 2001, 2007, 2013, 2014). However, determining the regional rainfall response to climate change is much more difficult and challenging (Chou et al. 2009; Bony et al. 2013; Kitoh et al. 2013; Krishnan et al. 2013). Specifically, assessing the potential impact of global climate change on the Asian summer monsoon (ASM) characteristics is a major concern, especially for the densely populated countries in south Asia, like India. This prompts for an imperative assessment of the ASM behaviour in the future changing climate, which is now recognised as a principal challenge for the whole scientific community.

Many previous studies (e.g. Meehl and Washington 1993; Bhaskaran et al. 1995; Douville et al. 2000, 2002; May 2002, 2004, 2011; Turner et al. 2007; Turner and Slingo 2009; Turner and Annamalai 2012) noted that greenhouse warming intensifies the monsoon precipitation over ASM region, particularly over Indo-Bay of Bengal region. A slight poleward shift and a weakening of the low-level monsoon circulation have also been suggested, leading to the so-called “monsoon paradox” (e.g. Turner et al. 2007; May 2004; Cherchi et al. 2011). Recent investigations using Coupled Model Intercomparison Project phase 5 (CMIP5) projections further confirm these inferences (e.g. Menon et al. 2013; Kitoh et al. 2013; Sandeep and Ajayamohan 2015; Sharmila et al. 2015; Sooraj et al. 2015). However, Ma and Yu (2014) and Ogata et al. (2014), using the same CMIP5 projections, highlight again this monsoon paradox with a strengthening of the ASM low-level circulation, but a weaker upper-level circulation. So, while consistent and repeated evidences are found for the future rainfall abundance under different CMIP projections (e.g. May 2002, 2004, 2011; IPCC 2001, 2007, 2013; Turner et al. 2007; Turner and Slingo 2009; Hsu et al. 2012;

Kitoh et al. 1997, 2013; Sooraj et al. 2015), contradictions still prevail for the ASM circulation changes (Ma and Yu 2014; Tanaka et al. 2005; Ueda et al. 2006). Recent ultra-high resolution atmospheric model simulations also show consistency in weakening of large-scale ASM overturning circulation in future projections (Ashfaq et al. 2009; Krishnan et al. 2013). However, these ultra-high resolution models also simulate decreasing summer precipitation over the Western Ghats, one of the key rainfall belts over the Indian monsoon region; the results of which are not consistent with the coarse CMIP5 projections (e.g. Sooraj et al. 2015; Sharmila et al. 2015). Adding further complexity to these, Kitoh et al. (2013) demonstrate strong sensitivity of ASM land rainfall relative to other regional monsoons in a global warming context. The specific reasons for all these discrepancies are not yet clear and hence the future ASM characteristics under global warming scenario remain intriguingly an open question, and still elude us.

The future changes in climate phenomena, such as El Niño Southern Oscillation (ENSO) or Indian Ocean Dipole Mode (IOD), can also modulate future ASM characteristics, as ENSO and IOD are tightly linked to ASM variability (Pillai and Annamalai 2012; Ashok et al. 2001; Ashok et al. 2004; Ummenhofer et al. 2011). Many studies have investigated these aspects (e.g. Ashrit et al. 2005; Yukimoto et al. 2006; Turner et al. 2007; Annamalai et al. 2007; Jourdain et al. 2013). For example, Annamalai et al. (2007) using selected CMIP3 models with a realistic representation of ENSO-monsoon relationship, showed increase in mean monsoon rainfall as well as an increase in interannual variability (by about 5%–10%, compared to the 20th century CMIP3 runs). Annamalai et al. (2007) additionally suggested that monsoon-ENSO relationship may not weaken under global warming scenario. Turner et al. (2007), using HadCM3 model configurations, also found that the teleconnection between ENSO and the ASM remains robust in the future climate. According to them, there is increased SST variability over east Pacific, which promotes an increase in monsoon

111 variability. Some other earlier studies also showed an increase in monsoon rainfall variability
112 in future climate (Hu et al. 2000; May 2004; Yukimoto et al. 2006). Recently, Jourdain et al.
113 (2013) have re-evaluated these aspects using a set of selected CMIP5 models, which show
114 limited biases with regard to monsoon-ENSO relationship. These selected CMIP5 models
115 also consistently produce significantly more summer rainfall over India and South Asian
116 region during the 21st century compared to the historical period. On interannual time scales,
117 contrary to the aforesaid results (e.g. Hu et al. 2000; May 2004; Yukimoto et al. 2006), they
118 found no significant changes in monsoon variability in most of these selected models.
119 Therefore, the lack of consensus among the models points that future projection of monsoon
120 variability also remains highly uncertain.

121 The aforementioned studies (e.g. Turner et al. 2007; Jourdain et al. 2013; Sandeep and
122 Ajayamohan 2015; Sooraj et al. 2015) deciphered future ASM changes using seasonal mean
123 precipitation. However, the finer temporal details of precipitation distribution, such as its
124 intensity and frequency (in other words daily rainfall extremes), are the most important
125 factors in determining the impacts of future changes in precipitation (Meehl et al. 2000;
126 Trenberth 2012). These finer details on rainfall changes cannot be inferred solely using
127 seasonal mean rainfall. Moreover, monsoon daily and intraseasonal variabilities influence the
128 seasonal mean through generation of internal variability and act as major building blocks for
129 ASM (Goswami et al. 2006a; Goswami and Xavier 2005). This, in turn, points to the
130 importance of rainfall frequency and intensity changes in deciphering the physical factors
131 responsible for the ASM trends in future projections. Supporting this argument, some
132 previous observational studies on ASM show that heavy daily precipitation events tend to
133 become more frequent (Goswami et al. 2006b; Rajeevan et al. 2008), while light to moderate
134 events become less frequent (Dash et al. 2009). Recently, Chou et al. (2012) made an attempt
135 to analyse future changes in precipitation characteristics (its intensity and frequency) over the

136 global tropics (30^0S-30^0N) and also provided possible mechanisms for these changes, using
137 CMIP3 models. However, how global warming exactly affects the ASM precipitation
138 characteristics is less known and the underlying mechanisms are not well understood. The
139 present study intends to address this aspect in the CMIP5 database, taking the intensity and
140 frequency of the future ASM rainfall changes into full consideration. As the intensity and
141 frequency changes can vary geographically as well, we also pay attention to the regional
142 features of future daily rainfall characteristics, concentrating specifically on the detailed
143 physical processes responsible for these changes.

144 Future changes in seasonal mean ASM rainfall have been studied in Sooraj et al.
145 (2015). The current work is a follow up of this study, extending it to the daily time scale, with
146 a particular focus on daily rainfall extremes. We aim to examine the future changes in
147 precipitation intensity and frequency over a large ASM region (50-110°E and 20°S-30°N),
148 where large-scale convection dominates with multiple regional rainfall maxima over the
149 eastern equatorial Indian Ocean and central India/north Bay of Bengal, respectively
150 (Annamalai and Sperber 2005). Our future assessment here basically unravels a north-south
151 rainfall dipole pattern positioned over these two regional rainfall centres and is found to occur
152 at both seasonal and sub-seasonal time scales in the CMIP5 projections. This peculiar robust
153 future change signature in a large set of CMIP5 models motivated further to explore the
154 detailed mechanisms that induced these changes. In particular, we focus on changes in
155 precipitation frequency and intensity, and their association with changes in seasonal mean
156 precipitation over ASM. We also aim to pursue the relative contributions of different
157 moisture budget components on the projected regional rainfall changes over ASM region, at
158 sub-seasonal time scale, to provide further insights on the governing physical processes.

159 The manuscript comprises the following sections. Section 2 includes data and
160 methodology, giving a brief description of the datasets and methodologies used in our

161 analysis. Section 3 presents the sub-seasonal aspects of monsoon response in climate change
162 experiments. Section 4 examines the possible mechanisms causing the future rainfall patterns.
163 Section 5 provides the discussion and summarizes the main conclusions from our study.

164 **2. Data and Methodology**

165 **2.1 Data used**

166 We use the historical and Representative Concentration Pathway (RCP) 4.5 climate
167 experiments from 32 Coupled General Circulation Models (CGCM) contributing to CMIP5
168 (Taylor et al. 2012; http://pcmdi9.llnl.gov). Table 1 provides the model details and
169 descriptions. Out of these 32, there are 12 (see red coloured ones in Table 1) models with the
170 necessary daily atmospheric circulation and precipitation fields for both historical and RCP
171 4.5 simulations available for a moisture budget analysis, at the time of our analysis. A
172 moisture budget analysis using a larger number of models is currently hampered by the non-
173 availability of all the necessary daily variables for many CMIP5 models. We also use these
174 selected models to further understand the detailed physical process causing the change in
175 rainfall pattern in future climate and to illustrate the inter-model spread in the CMIP5
176 database in the following sections.

177 The 20-year mean during 1980-1999 in historical simulations defines the present-day
178 climatology, the mean during 2080-2099 in RCP 4.5 defines the future climatology, and their
179 difference represents the future change under global warming. All the diagnostics are
180 performed only for the boreal summer season (June to September, JJAS hereafter). Note also
181 that we often use the term "sub-seasonal" throughout the manuscript. For avoiding any
182 confusion on its usage, it simply refers to analysis pertaining to daily rainfall.

183 We also use daily rainfall data from Tropical Rainfall Measuring Mission (TRMM
184 B42 version, Huffman et al. 2007). In the rest of the manuscript, "TRMM" refers to this
185 observed rainfall data. The period of analysis is from 1998 to 2009 for rainfall.

2.2 Diagnostic methods for daily rainfall distribution and extremes

As per recent studies (e.g. Kim et al. 2014), state-of-art climate models show a wide spread in simulating the precipitation intensities for the present-day climate and using absolute rainfall thresholds to a group of models may be problematic in distinctly capturing the precipitation strength, as the same precipitation intensity would correspond to a different percentile in different model simulations. In other words, future ASM assessments based on absolute rainfall thresholds may not be sufficient enough within the context of climate change projections. So relying on the spread information inherent in a set of models, here we employed percentile intensity estimates, to identify the daily rainfall extremes in each model separately. For each model (and also observation), the percentile values are calculated for JJAS period of every year and then averaged across the years for estimating the mean value for this particular model. The averaging is used here to eliminate the effects of interannual variations, which are not considered in this study. As an example, we show the computed rainfall intensities corresponding to 90, 95 and 99th percentiles for both observations (e.g. TRMM) and historical CMIP5 simulations in Figure 1. One can easily notice that the percentile estimates differ widely among the models, thus demonstrating systematic discrepancies in the precipitation intensities. For example, the rainfall intensity at 99th percentile is close to 25 mm day^{-1} in CanESM2 (denoted by CAN in Fig. 1), IPSL-CM5A-LR (denoted by IPLR) and BNU-ESM (denoted by BNU), whilst it is around 60 mm day^{-1} in BCC-CSM1.1 (see BCC in Fig. 1) and 40 mm day^{-1} in CCSM4 (see CCSM in Fig. 1). One can also see that while TRMM shows quite distinct values for 90 and 95th percentile estimates (22 and 34 mm day^{-1}, respectively), it is not the case in many models (CanESM2, GFDL-ESM-2G, GFDL-ESM-2M, GFDL-CM3, IPSL-CM5A-LR and IPSL-CM5A-MR). As an illustration, GFDL-ESM-2G has very comparable 90 and 95th percentile intensities equal to 15 and 18 mm day^{-1}, respectively. While other recent studies on future ASM climate (e.g.

211 Kitoh et al. 2013; Sharmila et al. 2015) used simple "absolute" threshold indices to define the
212 rainfall regimes in the current climate and percentage changes with respect to these absolute
213 thresholds to assess future change, our study, using percentile based thresholds, takes care of
214 the above systematic inconsistencies in the precipitation intensities in order to obtain more
215 robust results for future changes.

216 Taking account of this large inter-model spread in percentile estimates of precipitation
217 intensity among the models (as noted above in Fig. 1), the extreme events for each model are
218 estimated using their own respective percentile thresholds. Note also that the percentile
219 thresholds for each model are chosen based on their historical simulations, retaining the same
220 thresholds for RCP4.5 simulations to determine future changes. As noted above, the
221 percentile estimates for each model are calculated for JJAS period of every year, before
222 taking their final mean.

223 In our analysis of the daily rainfall time series of the 32 CMIP5 models listed in
224 Table 1, we use the following percentile thresholds to assess the daily rainfall distribution in
225 historical simulations and its future change in RCP4.5 simulations: 25, 75, 90, 95 and 99th
226 percentiles. Previous studies dealing on climate change extremes typically used only the 90th
227 percentile as a threshold for defining rainfall extremes (e.g. Moberg et al. 2006; IPCC 2007).
228 As our interest is also on the rainfall extremes, we decide to refine this top 10 % of the daily
229 rainfall distribution into further bins (90, 95 and 99th percentiles) in order to provide more
230 spatial details about very intense rainfall events (see Figures 2, 3 and 5 in the following
231 sections). Interestingly, it is found that the 99th percentile threshold shows much more inter-
232 model spread compared to the 90 and 95th percentiles in the CMIP5 database (see Fig. 1).

233 However, in order to simplify the discussion about the frequency/intensity of the
234 rainfall events and also the moisture budget analysis, when individual models are considered
235 (e.g. those in red in Table 1), only four precipitation regimes are identified: light, moderate,

heavy and heaviest rainfall events (see Figures 4 and 7-13 in the following sections). Light events are the rainfall events falling within the percentile thresholds of 1 to 25th. Similarly, moderate (heavy) events used a percentile threshold interval between 25 to 75th (75 to 95th) percentiles. Heaviest rainfall events are defined as rainfall events with intensity above the 95th percentile threshold. Similar type of percentile threshold analysis can be found in Lau and Wu (2007) and Allan and Soden (2008) for the global tropics, but they used slightly different percentile definitions. For calculating frequency in each rainfall regime, we simply count the number of days for each rainfall event in each category (as defined above) over the region of interest in the entire 20 year, for the JJAS season. Frequency will be expressed in percentage with respect to the total number of JJAS days. On the other hand, the rainfall intensity (in mm day^{-1}) is estimated by taking the average rainfall for each category.

Our analysis will focus specifically on extreme precipitation events (identified using the percentile threshold intensity method described above) over the North (60-110°E, 5-25°N) and South (80-110°E, 15°S-Equator) ASM regions (NASM and SASM, respectively, hereafter). These regions basically define the two important heat sources associated with ASM system (Annamalai and Sperber 2005). These regional rainfall centres are found to interact and influence each other on all time scales (Annamalai and Sperber 2005) and may play a vital role to determine the spatio-temporal structure of future ASM response. The reason for selecting these regions for further analysis will become evident as we proceed to the next section.

In order to further document the spatial variability of daily rainfall distributions over ASM domain in present-day and future climates, we also employed two classical statistics, namely skewness and kurtosis coefficients (von Storch and Zwiers 2001). These statistics are computed as

$$Skewness = \frac{nM3}{(n-1)(n-2)\sigma^3} \qquad (1)$$

$$Kurtosis = \frac{M4}{n\,\sigma^4} - 3 \qquad (2)$$

where n is the number of observations, $M3$ ($M4$) is equal to the sum of the deviations from the mean raised to the third (fourth) power and σ is the standard deviation.

Skewness measures the deviation of the distribution of a variable from symmetry. For a symmetrical distribution, the skewness coefficient is always equal to zero, but the converse is not true. Skewness is zero for a normal distribution. For unimodal distributions shifted to the right (left), the skewness coefficient is positive (negative). Kurtosis measures the flatness or peakedness of the distribution of a variable. The kurtosis coefficient is always greater or equal to -2 and is equal to zero for a normal distribution. In most cases, if the kurtosis is greater (lower) than zero then the distribution is more peaked (flatter) than the normal distribution with the same mean and standard-deviation. Extreme departures from the mean will cause very high values of kurtosis. Consequently, the kurtosis coefficient can be used to detect extreme observations or outliers in a sample of observations. These statistics are applied here to the unfiltered daily rainfall anomalies for each model. The daily anomalies (both the observed and simulated) are calculated by removing the annual cycle composed of the time mean and the first three Fourier harmonics. Finally, skewness and kurtosis statistics, computed separately for each model, are averaged across the models for both the RCP4.5 and historical simulations in order to obtain more robust results.

3. Changes in precipitation frequency and intensity

Figures 2a-f depict the ensemble seasonal mean rainfall pattern, along with spatial distributions of sub-seasonal percentile rainfall intensities in the simulated present-day monsoon climate using 32 CMIP5 models. As described earlier, in Figures 2b-f, the percentile rainfall intensities are calculated for each model, for each and every JJAS season, before averaging. The subsequent grand "ensemble mean" (using 32 models) is shown here. Figure 3 displays rainfall statistics from TRMM product using exactly the same method. The

observed seasonal mean rainfall pattern is realistically simulated by the ensemble mean (e.g. compare Figs. 2a and 3a), but with reduced intensity. Consistent with previous studies, the figures also suggest that ASM consists of multiple local rainfall maxima centred over the Bay of Bengal region, the tropical western Pacific and the eastern equatorial Indian Ocean (Annamalai and Sperber 2005; Annamalai and Liu 2005; Annamalai et al. 2007; Sooraj et al. 2015). The seasonal rainfall climatology of CMIP5 models and its biases have been recently documented (Sperber et al. 2013; Sooraj et al. 2015) and are not repeated here for conciseness.

Coming to the sub-seasonal patterns (Figs. 2b-f and 3b-f), the ensemble mean of CMIP5 models overestimates the observed rainfall intensities of lower tail events (which belong to light and moderate events), while underestimating those in the upper tail of the daily rainfall distribution, a common problem in many state-of-art climate models (e.g. Kim et al. 2014; Xavier 2012; Chou et al. 2012; Turner and Slingo 2009). Xavier (2012) while evaluating precipitation distribution in 14 CMIP3 climate models found that most models tend to reside in a light rainfall regime and the transition towards heavy precipitation is not as gradual as in the observations. In the observations (Figs. 3b-f), the contribution of lower tail rain intensities to the seasonal total rainfall appears to be small compared to those intensities above the 90^{th} percentile threshold. However for the model ensemble mean, there seems to be significant contributions from all the rainfall categories. All the aforementioned spatial features, particularly sub-seasonal analysis, are seen consistently across the individual models.

In order to illustrate this, Figure 4 displays the behaviour of the 12 selected models (e.g. those in red in Table 1; see Section 2.1 for further details) in simulating the daily rainfall characteristics over the two important regional heat source regions in the ASM domain (e.g. NASM and SASM). Note that we used here only these 12 individual models in order to be

consistent with our subsequent discussion using moisture budget estimates (see Section 4). In both domains, while precipitation intensity (see Figs. 4a-b) rises rapidly from moderate to heaviest rainfall events (see Section 2.2 for more details on rainfall categories and related definitions) reaching more than 20 mm day^{-1} in most of the models, the rainfall frequency (expressed in percentage, see Figs. 4c-d) decreases as the intensity increases from light to heaviest events as expected. Accordingly, light to moderate events are relatively more frequent in number compared to heavy and heaviest events. Furthermore, the distribution of precipitation intensity (see Figs. 4a-b) and frequency (expressed in percentage, see Figs. 4c-d) are generally similar in both domains, with slight exceptions in moderate rain frequency. But, if we look more carefully at Figures 4a-d, we observe that the models differ among themselves in simulating the finer details of the daily rainfall distributions. While all the models show marginal intensity biases for light to heavy rainfall events (see the TRMM column in Figs. 4a-b, for observations), there is relatively large model spread for the heaviest rainfall events, with almost all the models systematically underestimating the precipitation intensity of rainfall events above the 95^{th} percentile threshold. Most of the models also underestimate (overestimate) the frequency of light (moderate) events compared to observations (see Figs. 4c-d). It seems that the frequency of events in the lower tail is relatively less well captured compared to the frequency of upper tail events (heavy and heaviest events) in the coarse CMIP5 models. Recent ultra-high resolution (with 20 km horizontal resolution) atmospheric model simulations show more realistic representation of monsoon rainfall intensity and frequency (Krishnan et al. 2013), suggesting the importance of realistic representation of orography and convective processes for simulating the daily rainfall distribution over the Indian domain. This points towards the inadequacy of CMIP5 models (being coarser in resolution) in resolving the fine ASM precipitation features (Krishnan et al. 2013; Sperber et al. 2013; Sooraj et al. 2015) and to problems associated with

336 the interpolation of the rainfall time series from these models, which is required for
337 computing ensemble means.

338 We now focus on similar statistics computed from the RCP4.5 simulations. Figure 5
339 shows the spatial distribution of projected future rainfall changes for the seasonal mean and
340 for the percentiles of daily rainfall distribution. Note here that for each model, the percentiles
341 for the future climate simulations are derived independently of the percentiles estimated from
342 present-day simulations (using exactly by the same method as described in Section 2). The
343 future change of the percentiles is estimated for each model and, finally, the ensemble mean
344 of these differences is computed. Future changes at both the seasonal and sub-seasonal time
345 scales depict a significant north-south dipole-like pattern with increased rainfall over the
346 Indian subcontinent (e.g. NASM) extending into the western Pacific region and decreased
347 rainfall in southeastern Indian Ocean region coinciding with the oceanic convergence zone
348 (e.g. SASM). The subsequent domain oriented analysis using individual models will
349 demonstrate further the robustness of this dipole structure of future rainfall changes.

350 Interestingly, the aforementioned mean state rainfall changes are mainly associated
351 with future responses in the higher percentiles (e.g. above the 75^{th} percentile; see Figs. 5c-f)
352 and thus the more intense rainfall events, suggesting significant changes in the probability
353 distribution of daily rainfall in the ASM region and not only a uniform shift or change of the
354 mean rainfall.

355 To further assess these probability distributional aspects of future rainfall changes, we
356 examine the skewness and kurtosis statistics (see Section 2.2 for more details) in the
357 historical and RCP4.5 simulations. Figures 6a-b display the ensemble average skewness and
358 kurtosis computed from the 32 CMIP5 models and estimated from the daily rainfall
359 anomalies in the historical simulations. As expected, the daily rainfall distributions are not
360 Gaussian, but highly positively skewed over the whole ASM region in the present-day

climate with relatively lower values over the latitudes encompassing equatorial IO to Indian landmass and high values to its north and south. The maximum values over northwestern desert region, Pakistan and northwestern Australia are particularly notable. The kurtosis statistic (Fig. 6b) also shows highly positive values and similar spatial distribution, further highlighting the non-Gaussian nature of rainfall time series (recall that a Gaussian time series has a kurtosis of zero and a value greater than zero indicates a distribution more peaked than a Gaussian distribution with the same mean and standard-deviation). Furthermore, the extreme positive values of kurtosis over the northwest India-Pakistan region demonstrate the existence of "outliers" (e.g. very intense daily rainfall events) in the daily rainfall distribution simulated by some of the CMIP5 models in its historical simulations, despite the coarse resolution in most of the CMIP5 models.

In future climate, skewness shows remarkable increase over three regions: northwest Australia, SASM region along equatorial convergence zone and another one over the northwest India-Pakistan domain and western Arabian Sea (Fig. 6c). The kurtosis statistic also shows similar pattern of changes in RCP4.5 simulations, pointing to more frequent extreme flood events over both northwest Australia, western maritime continent and, to a lesser extent, the northwest India-Pakistan in future climate (Fig. 6d). The increase over the Pakistan dry region suggests the potential role of global warming in promoting flood episodes over this region in addition to other factors suggested in recent studies (Rasmussen et al. 2015; Priya et al. 2015). Skewness and kurtosis also show an increase over Indian Peninsula, Bangladesh and the core monsoon region in central Indian landmass (74.5-85°E, 16.5-26.5°N, see Figs. 6c and d). The results over the core monsoon region and the north Bay of Bengal are consistent with the observational study of Goswami et al. (2006b). These authors noted an increase in the frequency and intensity of extreme rainfall events using observational record over the same land region. Thus, several regions in the ASM domain

386 may witness severe and more frequent anomalous rainfall events according to the CMIP5
387 simulations.

388 An intriguing feature is that while both the statistics (skewness and kurtosis) are
389 increasing over the NASM and SASM regions in future climate (see Figs. 6c, d), future
390 changes in mean state show a dipole structure, with increased (decreased) rainfall over
391 NASM (SASM) as displayed in Figure 5. We thus now focus on the NASM and SASM
392 domains for a more detailed examination of future changes in precipitation intensity and
393 frequency, using the rainfall categories defined in section 2.2. This analysis will also enable
394 one to appreciate the spread of the individual models in simulating the future climate. First,
395 recall our earlier descriptions in section 2.2, sub-seasonal future changes associated with such
396 rainfall events over the two domains are again measured relative to the percentile thresholds,
397 solely derived from the present-day climate (again for each model on a season-to-season
398 basis). As noted above, here the detailed analysis using individual models is limited to 12
399 models, so as to be consistent with the moisture budget discussion in section 4.

400 Figures 7a and c present the future changes in rainfall intensity and frequency over
401 NASM, respectively. All models show seasonal rainfall intensification over NASM (as
402 already noted in Sooraj et al. 2015), with a relative increase ranging from 6 to 15% for the
403 individual models (see Fig. 7a). The projected changes in the intensity of light to heavy
404 events are mostly positive, but very modest relative to the historical runs (see Fig. 7a).
405 Furthermore, the frequency analysis (see Fig. 7c) suggests that the frequency of the light to
406 moderate events only slightly decrease, while heavy events do not show a uniform robust
407 change throughout the models. In contrast, the heaviest events show a large consensus among
408 the models in depicting a consistent and robust relative increase in their intensities (ranging
409 from 5 to 10%, see Fig. 7a) and frequencies (see Fig. 7c), in agreement with the increase of
410 seasonal rainfall. Consequently, for all the selected models, the projected increase in heaviest

411 events is largely greater than those of the aforementioned light to moderate events. So based
412 on this frequency and intensity analysis, the mean rainfall increase over NASM region is
413 mainly associated with heaviest rainfall events, whose intensity and frequency are projected
414 to increase significantly in the future climate.

415 In confirmation with the spatial pattern in Figure 5a, all models show a decrease in the
416 seasonal rainfall over SASM region, with a relative decrease ranging from 5 to 25% for
417 individual models (see Fig. 7b). On sub-seasonal time scale, the precipitation intensity
418 consistently weakens for moderate rainfall events in all the models (see Fig. 7b), thus
419 partially accounting for the mean rainfall suppression. Heavy rain events also show similar
420 tendency to decrease in intensity, but not as consistent and high as for moderate events.
421 Heavy events also show a significant decrease in frequency (with only IPSL-CM5A-LR
422 showing no robust changes, see Fig. 7d), while this frequency decrease is less consistent for
423 moderate events with individual models showing either marginally increase or decrease. An
424 interesting observation here is that heaviest events generally show the largest relative increase
425 in intensity with exceptions only in GFDL-CM3 and CSIRO-Mk3.6.0 (showing decreasing
426 tendency, see Fig. 7b). However, the heaviest events are consistently less frequent over the
427 SASM region in almost all the models, offsetting their increase in intensity as far as their
428 effect on the seasonal mean is concerned (see Figs. 7c-d). So the mean rainfall decrease over
429 SASM region is associated with changes involving multiple rainfall events, the relative
430 contribution of which varies from model to model. But some of the models (as described
431 above) show a certain consensus in suggesting that the seasonal mean changes are mainly
432 associated with a combined reduction in moderate and heavy rainfall intensities, despite of
433 the fact that the heaviest rainfall intensities tend to increase their strength in future for most of
434 the models, as pointed out above. Frequency analysis suggests that the mean rainfall decrease
435 may be related to the reduced frequency in heavy to heaviest rain events. All these results are

436 also fully consistent with the significant positive increase of both the skewness and kurtosis
437 over the SASM region in future climate as illustrated in Figures 6c-d.

438 In summary, the above analysis shows that there are distinctive differences in the
439 future changes of probability distribution of rainfall characteristics over two domains;
440 however the rainfall change over SASM is more complex to interpret, compared to NASM.
441 The detailed processes leading to these distinct future changes in rainfall characteristics need
442 further examination, as done in the next Section.

443 **4. Possible mechanisms for future changes in ASM daily rainfall characteristics**

444 Having seen the detailed sub-seasonal characteristics of the future rainfall response
445 over ASM system (as described in the previous section), here we will focus on the possible
446 physical processes causing the daily changes in rainfall intensity. Our approach involves the
447 application of vertically integrated water vapour budgets, to bring out the role of different
448 components (horizontal advection, vertical advection and evaporative fluxes) of the moisture
449 budget for the future change in monsoon rainfall. Subsequently, this can give insight into the
450 effect of various processes in contributing to the future intensification or weakening of
451 regional rainfall over ASM. Moisture budget method has been widely used in various recent
452 studies (e.g. Prasanna and Annamalai 2012; Pillai and Annamalai 2012; Xavier et al. 2014)
453 and equation (3) below is the appropriate formulation in the climate change context (Chou et
454 al. 2009, 2012),

455 $$P' = E' - \overline{\vec{V}' \cdot \nabla q'} - \overline{\omega' \partial_p q'} \qquad (3)$$

456 where the prime and the overbar denote future change and vertical integration through
457 the entire troposphere, respectively; P represents the precipitation, E the surface latent heat
458 fluxes, $\vec{V}$ the horizontal velocity vector, ω the vertical pressure velocity and q the specific
459 humidity. The specific humidity is converted into energy units (W m^{-2}), assuming that all the

460 latent heat of evaporation (L) is absorbed. Similarly, both E and P are converted into energy
461 units (W m^{-2}). On the right hand side of (3), the last two terms represent the future change in
462 moisture advection (horizontal) and moisture convergence, respectively.

463 The moisture budget estimates presented here are subjected to the following
464 constraints and approximations. The calculation of the moisture budget is not performed on
465 original atmospheric levels and at each time step for each model; rather it is done at
466 interpolated standard pressure levels and using daily outputs only. Also the budget estimates
467 are made over selected regional domains (NASM and SASM), rather than over the entire
468 tropics. All these factors may contribute to errors which may in turn affect the closure of the
469 moisture budget (Chou et al. 2012).

470 In Figures 8 and 9, we plot the individual terms of the moisture budget for the
471 present-day climate simulations over NASM and SASM, respectively. Note here that the
472 budget estimates are shown separately for each rainfall categories as defined in Section 2.2
473 and that the residual term of the moisture budget is also shown in each case. These residuals
474 represent various unresolved sub-grid scale processes, such as water vapour storage in the
475 atmosphere and surface boundary effects (Chou et al. 2012). Regarding balancing constraints
476 of the atmospheric moisture budget, Paula and Kummerow (2014) noted that balancing
477 global moisture budgets is a difficult task and this is even more challenging at regional scales.
478 However, for most of the models and all rainfall categories displayed in Figures 8 and 9,
479 residuals are generally smaller compared to the leading budget components, suggesting that
480 the above approximations and related errors may not drastically modify our major
481 conclusions.

482 In the present day-climate (see Figs. 8-9), it is evident that moist convergence is the
483 leading term of the moisture budget for heavy to heaviest rainfall events over the two
484 domains. On the other hand, over both domains, the positive contribution from moist

485 convergence in the moisture budget decreases progressively from heavy to light rainfall
486 events, turning out to be the same order as that of the residual term for moderate events and
487 always assuming negative contribution (and also greater than the residual term) for light
488 events. Interestingly, the contribution of evaporation in the moisture budget follows an
489 evolution, which is nearly opposite to the moisture convergence, since evaporation is the
490 leading term of the moisture budget for light to moderate rainfall events and becomes
491 progressively insignificant to account for the occurrence of more intense rainfall events
492 (especially for the heaviest ones). Finally, moisture advection assumes negative values (e.g.
493 dry advection) for all the rainfall categories and it is relatively smaller (larger) for the heavy
494 to heaviest (light to moderate) events (see Figs. 8-9). The role of moisture advection is thus to
495 reduce the rainfall intensity, especially for the light and moderate rainfall events over the two
496 domains.

497 For heaviest rain events over the two domains, it seems that evaporation and moisture
498 advection approximately cancel out each other, the residual term becoming eventually the
499 second most important term of the moisture budget (see Figs. 8d-9d). Our analysis further
500 reveals that both evaporation and moisture convergence contribute significantly to the
501 moderate rainfall events, with former one dominating the later. Finally, for light rainfall
502 events, as already noted above, the vertical and horizontal components of moisture budget
503 contribute to reduce significantly its intensity (see Figs. 8a-9a). The indication is that
504 convection might not be dominant process for the light rainfall events over the two domains
505 and other processes such as evaporation and boundary layer process could be more important,
506 consistent with previous studies (Chou et al. 2012).

507 The future changes in moisture budget terms are examined next. Note here that future
508 changes are not shown in percentage unlike earlier plots related to the rainfall intensity
509 changes (e.g. Figs. 7a, b). As future rainfall responses are of distinct nature in the regions of

510 interest (see section 3), their budget results are discussed separately. Firstly, for conciseness,
511 over NASM, we mainly focus on changes in heaviest rainfall events, which register a highly
512 significant increase in their intensity and frequency characteristics (as described in section 3),
513 to eventually become the main contributor to the future seasonal mean precipitation
514 enhancement (see Figs. 5 and 7a). For light to moderate events (figures not shown), our
515 analysis shows that only evaporation contributes positively to their marginal future increase
516 in all the models, with no substantial favourable role from moisture advection and
517 convergence. For heavy rainfall events, future changes in budget components vary from
518 model to model and hence no robust conclusion can be drawn (figures not shown).

519 For the heaviest events, as expected, the changes of the contribution due to moisture
520 convergence in the budget assume a similar distribution as that of rainfall intensity changes,
521 across the models (Fig. 10). Interestingly, in many models, it seems that moisture advection
522 injects dry air into NASM region, offsetting the rainfall intensification (except BNU-ESM
523 and IPSL-CM5A-MR), but this effect is too weak in order to counterbalance the strong
524 positive contribution from moisture convergence. There is an additional positive contribution
525 from evaporation as well for some models, but it is also smaller compared to the moisture
526 convergence contribution. Finally, the residual term is less than moisture convergence (the
527 one exception is CCSM4), but still larger than rest of the budget terms and so it additionally
528 contributes to rainfall changes in some of the models (exception in BCC-CSM1.1, CMCC-
529 CMS, IPSL-CM5A-LR, CSIRO-Mk3.6.0 and NorESM1-M).

530 We now focus on the SASM region, which experiences reduced seasonal rainfall in
531 future climate simulations (see Figs. 5a and 7b). Future changes in moisture budget for light
532 events are not discussed here due to negligible changes in their rainfall intensities (see Fig.
533 7b). For moderate events, both moisture advection and convergence components contribute to
534 its reduced rainfall intensity, which, as shown earlier, partially explains the seasonal rainfall

decrease in future climate (see Figs. 7b and 11a). However, the contribution of the moisture divergence seems more significant since it is more robust and of greater amplitude across the models. The residual term is also usually smaller than moisture divergence, but in some cases it still contributes to rainfall reduction in moderate rainfall events, with exceptions in BNU-ESM, CMCC-CMS, CCSM4, GFDL-ESM-2G, IPSL-CM5A-LR and CSIRO-Mk3.6.0. On the other hand, evaporative fluxes from equatorial IO (an open ocean basin with no land boundaries to act as barriers) are generally positive and contribute to enhance the rainfall intensity of the moderate events, thus offsetting partially the combined negative effects of the three other components of the budget.

As noted in Section 3, heavy rain events also show similar tendency to decrease in intensity over SASM. Moisture advection and convergence components are responsible for this reduced intensity in 5 models (see Fig. 11b, BCC-CSM1.1, CCSM4, GFDL-ESM-2M, GFDL-CM3 and CSIRO-Mk3.6.0), however the role of the moisture divergence seems to be more consistent and prominent, compared to its advection counterpart (e.g. moisture advection is positive for BCC-CSM1.1 and GFDL-CM3). The role of the residual term is also different from one model to another, assuming large values for some models and the contribution of the evaporative fluxes is usually small in most of the models. Moreover, the contributions of the different terms of the moisture budget exhibit much inter-model spread and switch sign across the models. So for heavy rainfall events over SASM domain, determining the robust features of the moisture budget, which contribute to the simulated changes for future climate, is more complicated because the residual terms are very large for some models.

In the case of heaviest rainfall events, most models show increased intensity over SASM domain (Fig. 11c), moisture convergence is again the main leading contributor to the moisture budget, with a positive effect for most models. The horizontal advection

(evaporation) component of the budget tends always to damp (enhance) the amplitude of the heaviest events over the SASM. But the amplitude of these terms is rather small and they cancel out each other, leading to the dominance of moisture convergence (see Fig. 11c). Note here that for GFDL-CM3 and CSIRO-Mk3.6.0, which show exceptional decrease in heaviest rainfall intensities, moisture convergence (with negative contribution) dominates the other terms, with a secondary contribution from horizontal advection.

Figures 12-13 further reconcile the contributing factors for the future changes in rainfall over ASM region. Figure 12a-f (Figure 13a-f) shows the vertical profile of future changes in specific humidity and vertical velocity, calculated for each rainfall event and each model, over NASM (SASM) regions, respectively. Again, light rainfall is not included here as its characteristics (intensity and frequency, see Fig. 7) show negligible change over both domains. The distribution of moisture changes looks indistinguishable in both domains and is very similar from one rainfall category to another, demonstrating an increase of vapour content in the lower troposphere (see Figs. 12a-c and Figs. 13a-c), as expected from the Clausius-Clapeyron equation. On the other hand, vertical velocity changes show strong spatial and intensity dependencies (see Figs. 12d-f and Figs. 13d-f). In Figures 12 and 13, we also included the mean vertical velocity profile in the present-day climate to ascertain its role and importance, and to further facilitate interpretation of future rainfall changes (see Figs. 12g-i and 13g-i). The characteristics of vertical motion remain identical over two domains with vertical motion assuming stronger magnitudes as precipitation intensity increases from moderate to heaviest. This statement remains true in the future climate, despite the changes described in Figs. 12d-f and 13d-f. Thus the vertical motion shows much intensity dependency over two domains, whereas it is not the case with mean humidity profile (figures not shown).

584 Figures 12a-c further ascertain that the general increase in rainfall over NASM is
585 driven mainly by increased moisture convergence, associated with the increased water vapour
586 in the atmosphere, directly related to global warming (Bony et al. 2013). However, Figures
587 12d-f imply reduced ascending motion over NASM and so it seems that the dynamic
588 component of moisture convergence associated with vertical motion changes in the RCP4.5
589 simulations shows a drying effect in most of the models. The reduced ascending motion is
590 consistent with the weakening of ASM circulation found in climate models (see Section 1,
591 Krishnan et al. 2013; Sooraj et al. 2015). Interestingly, the drying effect shows substantial
592 progression from moderate to heaviest intensities. Recalling our results in Section 3, the
593 heaviest rainfall events show pronounced increase (see Fig. 7a) despite this prominent drying
594 effect thus implying a paradoxical behaviour. This can be understood by carefully
595 interpreting Figures 12g-i, along with the changes depicted in Figure 12a-f. As mentioned
596 above, the mean vertical motion (see Figs. 12g-i) shows substantial strength in extreme
597 heaviest events, relative to moderate and heavy events. This pronounced strength in
598 climatological ascending motion, in conjunction with moisture changes (Fig. 12c), explains
599 this paradox, as this will promote strong moisture convergence in the lower troposphere (see
600 Fig. 10), and to eventually overcome the above drying effect. Note that the moisture
601 convergence, as discussed here, can also be interpreted as a manifestation of the moisture
602 changes acting on climatological ascending motion, in other words, a nonlinear relationship.
603 One can see from Figure 7a that GFDL-CM3 shows only a slight intensification for the
604 heaviest rainfall events compared to other models (see Fig. 7a) and Figure 12f clearly
605 demonstrates that this discrepancy is due to a pronounced relative reduction in vertical
606 motion and the resultant drying affect in this model. Again, the same drying effect (see Figs.
607 12d-e), with weaker mean ascending motion (see Figs. 12g-h) and the associated weaker
608 moisture convergence (figure not shown) may also explain the negligibly small changes in

609 moderate to heavy intensities (as shown in section 3, see Fig. 7a) as it may completely nullify
610 the moistening effect due to the increased moisture in the atmosphere (see Figs. 12a-b).
611 Over SASM region where there is seasonal rainfall suppression (see Fig. 7b), a
612 pronounced weakening of the ascending motion is found, especially for moderate to heavy
613 rainfall events (see Figs. 13d-e). This imparts a strong negative contribution to the moisture
614 convergence due to decreased vertical motion. Further as explained earlier, weaker
615 climatological ascending motion (relative to that of heaviest intensities, see Figs. 13g-i)
616 implies weaker moisture convergence and thus the interaction between these two processes
617 partially explains the significant reduced intensity in local moderate to heavy rainfall events
618 (see Fig. 7b). Note that the changes in vertical motion portray larger spread over SASM
619 compared to NASM, especially for heavy rainfall events (see Figs. 12e-13e). This may also
620 partially explain the significant model spread, as discussed early while describing the budget
621 terms for heavy rainfall intensity (see Fig. 11b). The implication is that the differences in
622 vertical velocity component may add discrepancy for changes in rainfall intensity among the
623 climate models, which may be attributed to the different cumulus parameterization used in
624 climate models (e.g. Chou et al. 2012).
625 As noted in the previous section, most models demonstrate increased intensity for
626 heaviest rainfall events over the SASM domain, despite mean rainfall suppression (see Fig.
627 7b). Figures 13c,i extend support to our earlier argument over NASM region, as the drying
628 effect (due to decreased vertical motion, see Fig. 13f) seems to be not strong enough, to
629 counterbalance the moisture convergence associated with moisture change and mean vertical
630 motion (see Figs. 11c, 13c and 13i). In Figure 7b, earlier we also noted reduced heaviest
631 rainfall intensity in GFDL-CM3 and CSIRO-Mk3.6.0. Figure 13f conspicuously further
632 supports our above argument on the adverse and key contribution of the vertical velocity
633 changes to the moisture convergence, as these two outlier models show a highly significant

weakening of upward motion compared to other models, thus accounting for the reduced intensity in their heaviest rainfall events.

As a last note to this section, our analysis shows that changes in moisture convergence are dominated by either changes in atmospheric water vapour content or changes in vertical motion, depending on the rainfall categories and the associated mean profile of vertical velocity. We also note that the mean climatological vertical velocity shows much intensity dependency compared to humidity, as the former one progresses to large values with increase in rainfall intensity. We see that the moisture convergence is usually dominated by the climatological vertical motion acting on the humidity changes and appears to play a critical role for deciphering the future rainfall intensities. In other words, changes in rainfall intensity are mainly determined by the interplay between all these processes.

5. Discussion and conclusion

The climate change pattern detected in this analysis at both the seasonal and sub-seasonal time scales reveals a north-south dipole-like structure, with increased rainfall over NASM region (on Indian subcontinent) extending into the western Pacific region and decreased rainfall over SASM along the equatorial oceanic convergence zone in the CMIP5 projections. This common spatial structure at both seasonal and daily time scales seems robust as it is detected using 32 CMIP5 models. Our study further infers that future daily rainfall changes are associated with more intense rainfall events (i.e. changes in the higher percentiles, above the 75^{th} percentile; see Figs 5c-f), suggesting significant changes in the probability distribution of daily rainfall over the ASM region and not a uniform change of the seasonal JJAS mean in the CMIP5 database.

Recently, Sooraj et al. (2015) and Sharmila et al. (2015) also obtained similar future rainfall patterns in seasonal mean ASM precipitation, using selected CMIP5 models that reasonably represent the present-day rainfall climatology over the ASM region. While their

659 rainfall pattern also identifies rainfall enhancement over NASM region, the rainfall
660 suppression over SASM is not so robust in their analysis. Those studies used a limited
661 number of models in their analysis, which probably may not be able to fully resolve this
662 peculiar rainfall signature (e.g. asymmetric pattern) in the future climate. Intriguingly
663 coinciding with these results, Srivastava and DelSole (2014) also found a similar asymmetric
664 rainfall structure using CMIP5 models, while trying to identify the dominant spatial-temporal
665 mode associated with future change in ASM variability. By applying discriminant analysis to
666 JJAS rainfall anomalies for two types of CMIP5 simulations (pre-industrial control and 21st
667 century runs), they concluded that future response is dominated by two dipole modes: one
668 oriented east-west across the maritime continent and other oriented north-south across the
669 ASM region. Interestingly in contrast to the rainfall increase over NASM region, Kitoh et al.
670 (2013) found the largest rainfall intensification over the western Arabian Sea while studying
671 global and regional monsoon in a changing climate. The reason for this discrepancy may be
672 due to the fact that Kitoh et al. (2013) used a longer monsoon season spanning from May to
673 September to define the northern hemisphere summer monsoon and future change is
674 calculated accordingly. On the other hand, the present study uses the JJAS season (see section
675 2.1) to define the ASM taking into account the following factors: firstly the rainfall season
676 over the regions encompassing Indian landmass begins in early June and secondly the
677 monsoon rainfall during May occurs mostly over the Ocean. So the rainfall pattern as
678 demonstrated in this study may not be directly comparable with their future rainfall patterns.

679 Our analysis using daily rainfall events (as defined in section 2.2) infers that there are
680 distinctive differences in the future changes of probability distribution of rainfall
681 characteristics over the two domains; however the rainfall change over SASM is more
682 complex to interpret, compared to NASM. We uniquely attribute the mean rainfall increase
683 over NASM region to heaviest rainfall events, the intensity and frequency of which show a

684 pronounced increase in future projections. Rainfall suppression over SASM shows
685 contributions from multiple rainfall events, but with large inter-model spread. However, some
686 of the models show a combined reduction in moderate and heavy rainfall intensities.
687 Interestingly, even for this subset of models, the intensity of heaviest rainfall events tends to
688 increase over SASM region.

689 Recently, Chou et al. (2012), when examining future changes in precipitation
690 characteristics over the entire tropics, using CMIP3 models, have noted that heaviest
691 precipitation events occur more frequently, while light to moderate rain events become less
692 frequent. This coincides with our inferences over NASM. In this regard, earlier Trenberth et
693 al. (2003) noted that increase in rainfall intensity needs to be compensated by decrease in
694 frequency (especially for light to moderate rainfall events). Our present findings support all
695 these previous results.

696 Our moisture budget inferences for NASM region are also broadly in agreement with
697 the results of recent studies, using approximated water vapour budgets (Bony et al. 2013;
698 Sooraj et al. 2015). Our study further substantiates their results using daily rainfall
699 characteristics (e.g. intensity and frequency). Over NASM region where there is future
700 rainfall abundance in CMIP5 simulations, they found competing effects of the
701 thermodynamic (moisture convergence) and dynamic processes (weakened monsoon
702 circulation). According to them, the former component prevailed over the later one and
703 explains the future rainfall intensification in the CMIP5 models. The interpretation is that the
704 offsetting dynamic processes are due to increase in dry static stability of the atmosphere,
705 which tends to reduce the ascending motion and, consequently, counteracts the rainfall
706 intensification. Substantiating their interpretation, the present diagnostics also demonstrate a
707 considerable offset due to the dynamic component, as moisture convergence due to vertical
708 motion shows a drying effect in most of the models, especially for moderate to heavy events

709 (Figures 12d-f). This weaker low-level moisture convergence due to weaker mean vertical
710 motion (as explained in section 4) probably explains the negligibly small changes in
711 moderate to heavy rainfall intensities over NASM region in future projection, despite of the
712 increased water vapor (see Fig 7a).

713 Recently, Lee and Wang (2014) while studying the future changes of intensity and
714 area of the global monsoon using CMIP5 model projection also noticed future increase in
715 rainfall over NASM and they attributed it to the significant moisture increase over this region
716 due to the enhanced cyclonic circulation dominating the Eurasia and North Africa, in the
717 future climate. The amplification of moisture, which is partly related to the thermodynamic
718 effect as discussed above, is consistent with those inferred by Sooraj et al. (2015).

719 For explaining the rainfall suppression over SASM region, Sooraj et al. (2015) argued
720 that, as the thermodynamic component is always positive over climatological ascending
721 regions, the contribution of dynamic component to total rainfall changes must be strongly
722 negative in order to have negative rainfall anomalies in future projections. They further
723 attributed this reduced ascending motion and rainfall suppression to dry air advection. Some
724 of the earlier studies (e.g., Chou et al. 2009; Chou et al. 2012) also showed similar argument
725 for convective-margin zones, while examining future changes in tropical precipitation using
726 CMIP3 models. In section 4, we show that dry air advection also adds to the rainfall
727 reduction over SASM region in addition to moisture divergence. More specifically, we found
728 that the dry advection effect in moderate rainfall events contributes significantly to the
729 overall rainfall suppression over SASM for some of the models (CMCC-CMS, CCSM4,
730 GFDL-ESM-2G, NorESM1-M, GFDL-ESM-2M and CSIRO-Mk3.6.0, see Fig 11a). Similar
731 results hold for heaviest rainfall events as well (i.e. for GFDL-CM3 and CSIRO-Mk3.6.0, see
732 Fig 11c). However, it should be noted that the contribution due to dry advection is not

consistent throughout the models, suggesting its relative importance is model dependent and more modest.

Recently, Srivastava and DelSole (2014), while explaining their results on future mean rainfall structure (as discussed above), argue that large-scale rainfall reduction over SASM (equatorial IO) is due to the sudden changes in the radiative balance of the atmosphere. According to them, global warming weakens the net atmospheric radiative cooling, which stabilizes the atmosphere eventually suppressing the ascending motion. On similar lines, earlier Bony et al. (2013) argued that the weaker net atmospheric radiative cooling, associated with the rising levels of carbon dioxide concentration, affects the strength of the vertical component of the atmospheric circulation. On the other hand, Stowasser et al. (2009), using GFDL CM2.1 (GFDL model version 2.1) coupled model projections, argued that the rainfall suppression over equatorial IO is related to the enhanced convection over equatorial western Pacific, which forces strong subsidence over eastern equatorial IO region. The relative role of all these different processes is debatable and needs further investigation.

It is generally believed that current coarse climate models do not capture well the precipitation frequency and intensity, particularly for rainfall extremes (e.g. Allan and Soden 2007, 2008; Chou et al. 2007, 2012); a conclusion which is supported by our current diagnostics as well (see section 3). A few recent studies have reported important deficiencies in CMIP5 models and their inability to simulate the ASM Rainfall at different time scales due to coarse resolution or improper convection parameterization (Saha et al. 2014; Sabeerali et al. 2015). Some other studies, using time slice experiments and very high resolution or regional AGCMs suggest that Indian summer monsoon rainfall will decrease in future climate in contradictions with the results using CMIP5 models (Ashfaq et al. 2009; Krishnan et al. 2013). Thus, present global climate models may not be the best tool for assessing the regional rainfall changes (with proper sign and amplitude) in the future climate due to the important

role of the detailed changes of the vertical motion profiles on the rainfall intensity changes, as highlighted in this study. A natural extension of this work is thus to assess if the future daily rainfall changes documented here are also seen in the regional simulations produced in the framework of the ongoing Coordinated Regional Downscaling Experiment (CORDEX South-Asia, http://cccr.tropmet.res.in). However, in all the CMIP5 models, which we analysed, significant increase in heaviest rainfall events is projected in contrast to light to moderate events over NASM region (see section 3). The increase is also noted over northwest India and Pakistan, which already experienced several severe flood events in the last decade (Priya et al. 2015). So, despite the model caveats, the broader consensus within the models is noteworthy.

The extreme daily rainfall events as discussed in this study (see section 3) are inevitably important for ASM system; however ASM rainfall exhibits significant interannual fluctuations (with a standard deviation of about 9 cm day^{-1}), thus creating large-scale and persistent droughts or wet conditions, modulating the local daily rainfall distributions over India (e.g. Webster et al. 1998; Goswami and Ajayamohan 2001; Pillai and Annamalai 2012; Sharmila et al. 2015). Recently, Sharmila et al. (2015) using selected CMIP5 models speculated that severity of extended drought and wet events might also increase notably in future climate. So specific consideration needs to be given to the projected daily rainfall changes over the ASM region during anomalous monsoon years. The present work has not addressed this aspect. As a future work, we wish to examine the mean and distribution changes of daily rainfall in this context, by assessing how the daily rainfall probability distribution may be modified specifically during the extreme monsoon years at the interannual time scale (i.e. strong and weak monsoon years) in the future climate.

The rainfall within the monsoon season also possesses variation spanning synoptic to intraseasonal time scales, thus creating spells of active and break events often lasting a few

783 days to weeks (e.g. Goswami and Ajayamohan 2001; Annamalai and Slingo 2001; Turner
784 and Slingo 2009; Goswami et al. 2006a). Duration, intensity and frequency of these
785 active/break events contribute to the seasonal mean (e.g. Goswami and Ajayamohan, 2001;
786 Sperber et al. 2000). So, future changes of the temporal properties of these sub-seasonal
787 events could also have a vital impact on agricultural practices such as sowing and seeding of
788 crops. The precise impact of global warming on the active-break statistics remains unknown,
789 and is also a challenging problem for future research.
790

Acknowledgements

We sincerely thank Dr. Rajeevan M, Director, Indian Institute of Tropical Meteorology, India for all the support for this research study. We are also thankful to Drs Krishnan R and Mujumdar M for their valuable support in carrying out this research work. Pascal Terray is funded by Institut de Recherche pour le Développement (IRD, France) and this work was done while Pascal Terray was a visiting scientist at IITM. P. Xavier is supported by the Joint DECC/Defra Met Office Hadley Centre Climate Programme (GA01101). We acknowledge the climate modelling groups, the Program for Climate Model Diagnosis and Intercomparison, and the World Climate Research Programme's working Group on coupled modelling, for making available the "CMIP5" multi-model data sets. We also thank the anonymous reviewers for their constructive comments.

References

Allan RP, Soden BJ (2007) Large discrepancy between observed and simulated precipitation trends in the ascending and descending branches of the tropical circulation. Geophys Res Lett 34:L18705. doi:10.1029/2007GL031460

Allan RP, Soden BJ (2008) Atmospheric warming and the amplification of precipitation extremes. Science 321:1481–1484

Annamalai H, Liu P (2005) Response of the Asian Summer Monsoon to changes in El Niño properties. Q J R Meteorol Soc 131:805–831

Annamalai H, Slingo JM (2001) Active/break cycles: Diagnosis of the intraseasonal variability of the Asian summer monsoon. Clim Dyn 18:85–102.

Annamalai H, Sperber KR (2005) Regional heat sources and the active and break phases of boreal summer intraseasonal (30–50 day) variability. J Atmos Sci 62: 2726–2748

Annamalai H, Hamilton K, Sperber KR (2007) The South Asian summer monsoon and its relationship with ENSO in the IPCC AR4 simulations. J Clim 20:1071–1092

Ashfaq M, Shi Y, Tung WM, Trapp RJ, Gao X, Pal JS, Diffenbaugh NS (2009) Suppression of south Asian summer monsoon precipitation in the 21st century. Geophys Res Lett 36: L01704. doi:10.1029/2008GL036500

Ashok K, Guan Z, Saji NH, Yamagata T (2004) Individual and combined influences of ENSO and the Indian Ocean dipole on the Indian summer monsoon. J Clim 17(16):3141–3155

Ashok K, Guan Z, Yamagata T (2001) Impact of the Indian Ocean dipole on the relationship between the Indian monsoon rainfall and ENSO. Geophys Res Lett 28(23):4499–4502

Ashrit RG, Kitoh A, Yukimoto S (2005) Transient response of ENSO–monsoon teleconnection in MRI-CGCM2.2 climate change simulations. J Meteorol Soc Jpn 83: 273–291

828 Bhaskaran B, Mitchell JFB, Lavery JR, Lal M (1995) Climatic response of the Indian
829 subcontinent to doubled CO_2 concentration. Int J Climatol 15:873–892
830 Bony S, Bellon G, Klocke D, Sherwood S, Fermepin S, Denvil S (2013) Robust direct effect
831 of carbon dioxide on tropical circulation and regional precipitation. Nature Geosci
832 6:447–451
833 Cherchi A, Alessandri A, Masina S, Navarra A (2011) Effects of increased CO_2 on
834 monsoons. Clim Dyn 37:83–101. doi:10.1007/s00382-010-0801-7
835 Chou C, Tu JY, Tan PH (2007) Asymmetry of tropical precipitation change under global
836 warming. Geophys Res Lett 34:L17708. doi:10.1029/2007GL030327
837 Chou C, Neelin JD, Chen CA, Tu JY (2009) Evaluating the "rich-get-richer" mechanism in
838 tropical precipitation change under global warming. J Clim 22:1982–2005
839 Chou C, Chen CA, Tan PH, Chen KT (2012) Mechanisms for Global Warming Impacts on
840 Precipitation Frequency and Intensity. J Clim 25:3291–3306
841 Dash SK, Kulkarni MA, Mohanty UC, Prasad K (2009) Changes in the characteristics of rain
842 events in India. J Geophys Res 114:D10109
843 Douville H, Chauvin F, Planton S, Royer JF, Salas-Melia D, Tyteca S (2002) Sensitivity of
844 the hydrological cycle to increasing amounts of greenhouse gases and aerosols. Clim
845 Dyn 20:45–68
846 Douville H, Royer JF, Polcher J, Cox P, Gedney N, Stephenson DB, Valdes PJ (2000) Impact
847 of doubling CO_2 on the Asian summer monsoon: robust versus model-dependent
848 responses. J Meteorol Soc Jpn 78:421–439
849 Goswami BN, Ajayamohan RS (2001) Intraseasonal oscillations and interannual variability
850 of the Indian summer monsoon. J Clim 14:1180–1198
851 Goswami BN, Xavier PK (2005) Dynamics of 'Internal' interannual variability of Indian
852 Summer Monsoon in a GCM. J Geophys Res 110:D24104

853 Goswami BN, Wu G, Yasunari T (2006a) The annual cycle, intraseasonal oscillations and
854 roadblock to seasonal predictability of the Asian summer monsoon. J Clim 19:5078–
855 5099
856 Goswami BN, Venugopal V, Sengupta D, Madhusoodanan MS, Xavier PK (2006b)
857 Increasing Trend of Extreme Rain Events Over India in a Warming Environment.
858 Science 314:1442–1445
859 Hsu PC, Li T, Luo JJ, Murakami H, Kitoh A, Zhao M (2012) Increase of global monsoon
860 area and precipitation under global warming: a robust signal? Geophys Res Lett
861 39:L0670. doi:10.1029/2012GL051037
862 Hu ZZ, Latif M, Roeckner E, Bengtsson L (2000) Intensified Asian summer monsoon and its
863 variability in a coupled model forced by increasing greenhouse gas concentrations.
864 Geophys Res Lett 27:2681–2684
865 Huffman GJ, Adler RF, Bolvin DT, Gu G, Nelkin EJ, Bowman KP, Hong Y, Stocker EF,
866 Wolff DB (2007) The TRMM Multi-satellite precipitation analysis: quasi global, multi-
867 year, combined-sensor precipitation estimates at fine scale. J Hydrometeor 8:38–55
868 IPCC (2001) Third Assessment Report of the Intergovernmental Panel on Climate Change,
869 www.ipcc.ch/ipccreports/ar4-wg1.htm
870 IPCC (2007) Fourth Assessment Report of the Intergovernmental Panel on Climate Change,
871 www.ipcc.ch/ipccreports/ar4-wg1.htm
872 IPCC (2013) Fifth Assessment Report of the Intergovernmental Panel on Climate Change,
873 www.ipcc.ch/ipccreports/ar4-wg1.htm
874 IPCC (2014) Fifth Assessment Report of the Intergovernmental Panel on Climate Change,
875 www.ipcc.ch/ipccreports/ar4-wg1.htm

876 Jourdain NC, Gupta AS, Taschetto AS, Ummenhofer CC, Moise AF, Ashok K (2013) The
877 Indo-Australian monsoon and its relationship to ENSO and IOD in reanalysis data and
878 the CMIP3/CMIP5 simulations. Clim Dyn. doi:10.1007/s00382-013-1676-1
879 Kim D, co-authors (2014) Process-Oriented MJO Simulation Diagnostic: Moisture
880 Sensitivity of Simulated Convection. J Clim 27:5379–5395
881 Kitoh A, Yukimoto S, Noda A, Motoi T (1997) Simulated changes in the Asian summer
882 monsoon at times of increased atmospheric CO_2. J Meteorol Soc Jpn 75:1019–1031
883 Kitoh A, Endo H, Krishna Kumar K, Cavalcanti IFA, Goswami P, Zhou T (2013) Monsoons
884 in a changing world: A regional perspective in a global context. J Geophys Res 118:
885 3053–3065
886 Krishnan R**,** Sabin TP, Ayantika DC, Sugi M, Kitoh A, Murakami H, Turner A, Slingo JM,
887 Rajendran K (2013) Will the South Asian monsoon overturning circulation stabilize any
888 further? Clim Dyn doi:10.1007/s00382-012-1317-0
889 Lau KM, Wu HT (2007) Detecting trends in tropical rainfall characteristics, 1979–2003. Int J
890 Climatol 27:979–988
891 Lee JY, Wang B (2014) Future change of global monsoon in the CMIP5. Clim Dyn 42:101–
892 119. doi:10.1007/s00382-012-1564-0
893 Ma J, Yu JY (2014) Paradox in the South Asian summer monsoon circulation change: Lower
894 tropospheric strengthening and upper troposheric weakening. Geophys Res Lett 41.
895 doi: 10.1002/2014GL059891
896 May W (2002) Simulated changes of the Indian summer monsoon under enhanced
897 greenhouse gas conditions in a global time-slice experiment. Geophys Res Lett 29.
898 doi:10.1029/2001GL013808

May W (2004) Simulation of the variability and extremes of daily rainfall during the Indian summer monsoon for present and future times in a global time-slice experiment. Clim Dyn 22:183–204

May W (2011) The sensitivity of the Indian summer monsoon to a global warming of 2°C with respect to pre-industrial times. Clim Dyn 37:1843-1868. doi:10.1007/s00382-010-0942-8

Meehl GA, Washington WM (1993) South Asian summer monsoon variability in a model with a doubled atmospheric carbon-dioxide concentration. Science 260:1101–1104

Meehl GA, Zwiers F, Evans J, Knutson T, Mearns L, Whetton P (2000) Trends in extreme weather and climate events: issues related to modelling extremes in projections of future climate change. Bull Am Me Soc 81:427–436

Menon A, Levermann A, Schewe J, Lehmann J, Frieler K (2013) Consistent increase in Indian monsoon rainfall and its variability across CMIP-5 models. Earth Syst Dynam Discuss 4:287–300. doi:10.5194/esdd-4-287-2013

Moberg A, co-authors (2006) Indices for daily temperature and precipitation extremes in Europe analyzed for the period 1901–2000. J Geophys Res 111 (D22). doi:10.1029/2006JD007103

Ogata T, Ueda H, Inoue T, Hayasaki M, Yoshida A, Watanabe S, Kira M, Ooshiro M, Kumai A (2014) Projected Future Changes of the Asian Monsoon: A Comparison of CMIP3 and CMIP5 model results. J Meteorol Soc Jpn 92:207–225

Paula JB, Kummerow CD (2014) An Assessment of Atmospheric Water Budget Components over Tropical Oceans. J Clim 27:2054–2071

Pillai PA, Annamalai H (2012) Moist dynamics of severe monsoons over South Asia: Role of the tropical SST. J Atmos Sci 69:97–115

923 Prasanna V, Annamalai H (2012) Moist dynamics of extended monsoon breaks over South
924 Asia. J Clim 25:3810–3831
925 Priya P, Mujumdar M, Sabin TP, Terray P, Krishnan R (2015) Impacts of Indo-Pacific sea
926 surface temperature anomalies on the summer monsoon circulation and heavy
927 precipitation over northwest India-Pakistan region during 2010. J Clim 28:3714–3730.
928 doi: 10.1175/JCLI-D-14-00595.1
929 Rajeevan M, Bhate J, Jaswal AK (2008) Analysis of variability and trends of extreme
930 rainfall events over India using 104 years of gridded daily rainfall data. Geophys Res
931 Lett 35:L18707. doi: 10.1029/2008GL035143
932 Rasmussen KL, Hill AJ, Toma VE, Zuluaga MD, Webster PJ, Houze Jr RA (2015)
933 Multiscale analysis of three consecutive years of anomalous flooding in Pakistan. Q J R
934 Meteorol Soc 141:1259–1276. doi: 10.1002/qj.2433
935 Sabeerali C, Rao SA, Dhakate A, Salunke K, Goswami B (2015) Why ensemble mean
936 projection of south Asian monsoon rainfall by CMIP5 models is not reliable? Clim Dyn
937 45:161-174
938 Saha A, Ghosh S, Sahana AS, Rao EP (2014) Failure of CMIP5 climate models in simulating
939 post-1950 decreasing trend of Indian monsoon. Geophys Res Lett 41:7323-7330.
940 doi:10.1002/2014GL061573
941 Sandeep S, Ajaya Mohan RS (2015) Poleward shift in Indian summer monsoon low level
942 Jetstream under global warming. Clim Dyn 45:337–351. doi 10.1007/s00382-014-2261-
943 y
944 Sharmila S, Joseph S, Sahai AK, Abhilash S, Chattopadhyay R (2015) Future projection of
945 Indian summer monsoon variability under climate change scenario: An assessment
946 from CMIP5 climate models. Glob Planet Chang 124:62–78

947 Sooraj KP, Terray P, Mujumdar M (2015) Global warming and the weakening of the Asian
948 summer monsoon circulation: Assessments from the CMIP5 models. Clim Dyn
949 45:233–252. doi:10.1007/s00382-014-2257-7
950 Sperber KR, Slingo JM, Annamalai H (2000) Predictability and the relationship between
951 subseasonal and interannual variability during the Asian summer monsoons. Q J R
952 Meteorol Soc 126:2545–2574
953 Sperber KR, Annamalai H, Kang IS, Kitoh A, Moise A, Turner AG, Wang B, Zhou T (2013)
954 The Asian summer monsoon: An intercomparison of CMIP5 vs. CMIP3 simulations of
955 the late 20th century. Clim Dyn 41:2711-2744. doi:10.1007/s00382-012-1607-6
956 Srivastava A, DelSole T (2014) Robust Forced Response in South Asian Summer Monsoon
957 in a Future Climate. J Clim 27:7849–7860
958 Stowasser M, Annamalai H, Hafner J (2009) Response of the South Asian summer monsoon
959 to global warming: mean and synoptic systems. J Clim 22:1014–1036
960 Tanaka HL, Ishizaki N, Nohara D (2005) Intercomparison of the intensities and trends of
961 Hadley, Walker and monsoon circulations in the global warming projections. Sci Online
962 Lett Atmos 1:77–80. doi:10.2151/sola.2005-021
963 Taylor KE, Stouffer RJ, Meehl GA (2012) An overview of CMIP5 and the experiment
964 design. Bull Amer Meteor Soc 93:485–498
965 Trenberth KE (2012) Framing the way to relate climate extremes to climate change. Climatic
966 Change 115(2):283–290. doi:10.1007/s10584-012-0441-5
967 Trenberth KE, Dai A, Rasmussen RM, Parsons DB (2003) The changing character of
968 precipitation. Bull Amer Meteor Soc 84:1205–1217 doi:10.1175/BAMS-84-9-1205.
969 Turner AG, Annamalai H (2012) Climate change and the South Asian summer monsoon.
970 Nature Clim Change. doi:10.1038/NCLIMATE1495

971 Turner AG, Slingo JM (2009) Uncertainties in future projections of extreme precipitation in
972 the Indian monsoon region. Atmos Sci Lett 10:152–158. doi:10.1002/asl.223
973 Turner AG, Inness PM, Slingo JM (2007) The effect of doubled CO_2 and model basic state
974 biases on the monsoon-ENSO system. I: mean response and interannual variability.
975 QJR Meteorol Soc 133:1143–1157
976 Ueda H, Iwai A, Kuwako K, Hori ME (2006) Impact of anthropogenic forcing on the Asian
977 summer monsoon as simulated by eight GCMs. Geophys Res Lett 33:L06703.
978 doi:10.1029/2005GL025336
979 Ummenhofer CC, Sen Gupta A, Li Y, Taschetto AS, England MH (2011) Multi-decadal
980 modulation of the El Nino–Indian monsoon relationship by Indian Ocean variability.
981 Environ Res Lett 6:034006
982 Von Storch H, Zwiers FW (2001) Statistical Analysis in Climate Research. Cambridge
983 Univesity press. Cambridge UK. Chapter 13. 484 pp.
984 Webster PJ, Magaña VO, Palmer TN, Shukla J, Tomas RA, Yanai M, Yasunari T (1998)
985 Monsoons: Processes, predictability, and the prospects for prediction. J Geophys Res
986 103:14451–14510
987 Xavier PK (2012) Intraseasonal convective moistening in CMIP3 models. J Clim 25:2569–
988 2577
989 Xavier PK, Raizan R, Wee KC, Emily W (2014) Influence of Madden-Julian Oscillation on
990 South East Asia rainfall extremes - Observations and predictability. Geophys Res Lett
991 41:4406–4412. doi:10.1002/2014GL060241
992 Yukimoto S, Noda A, Uchiyama T, Kusunoki S (2006) Climate change of the twentieth
993 through twenty-first centuries simulated by MRI-CGCM2.3. Pap Meteor Geophys 56:
994 9–24
995

996 **Figure Captions**

997 Fig 1: Percentile rainfall intensity for daily time series over the ASM region (60-110°E and
998 15°S-25°N) from TRMM and historical simulations for selected CMIP5 models. Here BCC
999 stands for BCC-CSM1.1, similarly CMS for CMCC-CMS, BNU for BNU-ESM, CAN for
1000 CanESM2, CCSM for CCSM4, GF2G for GFDL-ESM-2G, GF2M for GFDL-ESM-2M,
1001 GFCM for GFDL-CM3, IPLR for IPSL-CM5A-LR, IPMR for IPSL-CM5A-MR, CSIR for
1002 CSIRO-Mk3.6.0, and finally NOR for NorESM1-M. Note that a log scale is used for the
1003 vertical axis and that the unit for this axis is in mm day^{-1}.

1004 **Figure 2:** (a) Ensemble mean rainfall (in mm day^{-1}) at seasonal time scale (for JJAS period)
1005 for historical simulations using 32 CMIP5 models. (b) to (f) Ensemble mean of rainfall
1006 intensities (in mm day^{-1}) at different percentile thresholds using daily rainfall from historical
1007 simulations of 32 CMIP5 models, for the JJAS period. See Section 2 for further details about
1008 the percentile thresholds definitions.

1009 **Figure 3:** Same as Fig 2, but for TRMM rainfall observations.

1010 **Figure 4a-d:** Rainfall intensity of various rainfall events over (a) NASM and (b) SASM
1011 domains, for historical simulations using 12 CMIP5 models. (c) and (d) are same as (a) and
1012 (b), but for rainfall frequency. Here BCC stands for BCC-CSM1.1, similarly CMS for
1013 CMCC-CMS, BNU for BNU-ESM, CAN for CanESM2, CCSM for CCSM4, GF2G for
1014 GFDL-ESM-2G, GF2M for GFDL-ESM-2M, GFCM for GFDL-CM3, IPLR for IPSL-
1015 CM5A-LR, IPMR for IPSL-CM5A-MR, CSIR for CSIRO-Mk3.6.0, and, finally, NOR for
1016 NorESM1-M. The unit for intensity is in mm day^{-1}, while for frequency, it is in percentages.

1017 **Figure 5:** Same as that of Figure 2, but for the future rainfall changes. As explained in the
1018 text, the rainfall intensities at various percentile thresholds are derived independently for the
1019 historical and RCP4.5 simulations and future change is finally calculated. See the text for
1020 more details. Stippling denotes the regions of statistically significant values at the 90%

confidence level, using a two tailed student *t*-test for the differences of means using a number of degrees of freedom (DOF) of 62 (e.g. DOF=2×number of models - 2). In other words, each model is assumed to be an independent observation for computing the *t*-statistic. Color shading represents the future changes values, without applying any significance test. The thick black contour is the zero isoline.

Figure 6: Ensemble mean patterns and their future changes for Kurtosis (a and c) and Skewness (b and d) statistics of rainfall distribution, using 32 CMIP5 models. (a) and (b) for present-day climate. (c) and (d) for future change, expressed in percentages.

Figure 7a-d: Future change in rainfall intensity (in %) of various rainfall events over (a) NASM and (b) SASM domains. In (c) and (d), same as (a) and (b), but for rainfall frequency (in %). Here BCC stands for BCC-CSM1.1, similarly CMS for CMCC-CMS, BNU for BNU-ESM, CAN for CanESM2, CCSM for CCSM4, GF2G for GFDL-ESM-2G, GF2M for GFDL-ESM-2M, GFCM for GFDL-CM3, IPLR for IPSL-CM5A-LR, IPMR for IPSL-CM5A-MR, CSIR for CSIRO-Mk3.6.0, and, finally, NOR for NorESM1-M.

Figure 8a-d: Moisture Budget terms (in W m^{-2}) over NASM region for the present-day climate, as calculated for various rainfall events. MoiCon represents moisture convergence, MoiAdv is for moisture advection, Evap is for evaporation and Res stands for budget residual term. Here BCC stands for BCC-CSM1.1, similarly CMS for CMCC-CMS, BNU for BNU-ESM, CAN for CanESM2, CCSM for CCSM4, GF2G for GFDL-ESM-2G, GF2M for GFDL-ESM-2M, GFCM for GFDL-CM3, IPLR for IPSL-CM5A-LR, IPMR for IPSL-CM5A-MR, CSIR for CSIRO-Mk3.6.0, and, finally, NOR for NorESM1-M.

Figure 9a-d: Moisture Budget terms (in W m^{-2}) over SASM region for the present-day climate, as calculated for various rainfall events. MoiCon represents moisture convergence, MoiAdv is for moisture advection, Evap is for evaporation and Res stands for budget residual term. Here BCC stands for BCC-CSM1.1, similarly CMS for CMCC-CMS, BNU for BNU-

ESM, CAN for CanESM2, CCSM for CCSM4, GF2G for GFDL-ESM-2G, GF2M for GFDL-ESM-2M, GFCM for GFDL-CM3, IPLR for IPSL-CM5A-LR, IPMR for IPSL-CM5A-MR, CSIR for CSIRO-Mk3.6.0, and, finally, NOR for NorESM1-M.

Figure 10: Future changes in moisture Budget terms (in W m^{-2}) over NASM region as calculated for heaviest rainfall intensities. MoiCon represents moisture convergence, MoiAdv is for moisture advection, Evap is for evaporation and Res stands for budget residual term. Here, BCC stands for BCC-CSM1.1, similarly, CMS for CMCC-CMS, BNU for BNU-ESM, CAN for CanESM2, CCSM for CCSM4, GF2G for GFDL-ESM-2G, GF2M for GFDL-ESM-2M, GFCM for GFDL-CM3, IPLR for IPSL-CM5A-LR, IPMR for IPSL-CM5A-MR, CSIR for CSIRO-Mk3.6.0, and, finally, NOR for NorESM1-M.

Figure 11a-c: Future changes in moisture Budget terms (in W m^{-2}) over SASM region as calculated for various rainfall events. MoiCon represents moisture convergence, MoiAdv is for moisture advection, Evap is for evaporation and Res stands for budget residual term. Here, BCC stands for BCC-CSM1.1, similarly CMS for CMCC-CMS, BNU for BNU-ESM, CAN for CanESM2, CCSM for CCSM4, GF2G for GFDL-ESM-2G, GF2M for GFDL-ESM-2M, GFCM for GFDL-CM3, IPLR for IPSL-CM5A-LR, IPMR for IPSL-CM5A-MR, CSIR for CSIRO-Mk3.6.0, and, finally, NOR for NorESM1-M.

Figure 12a-f: (a)-(f) Vertical profiles of future change in specific humidity (left panels, $\times 10^{-3}$ kg kg^{-1}) and vertical component of velocity (middle panels, $\times$-10^{-2} Pa s^{-1}) over NASM, as calculated for various rainfall events in 12 selected CMIP5 models. (g)-(i) Mean vertical profiles of vertical component of velocity (unit is -10^{-2} Pa s^{-1}) computed from historical simulations of the same 12 CMIP5 models, for various rainfall events over NASM.

Figure 13a-f: (a)-(f) Vertical profiles of future change in specific humidity (left panels, $\times 10^{-3}$ kg kg^{-1}) and vertical component of velocity (middle panels, $\times$-10^{-2} Pa s^{-1}) over SASM, as calculated for various rainfall events in 12 selected CMIP5 models. (g)-(i) Mean vertical

1071 profiles of vertical component of velocity (unit is -10^{-2} Pa s^{-1}) computed from historical

1072 simulations of the same 12 CMIP5 models, for various rainfall events over SASM.

1073

Table Captions:

Table 1: Description of the 32 CMIP5 models used in our analysis. The 12 models shown in red are those used for our detailed analysis and those having all the necessary daily atmospheric circulation and precipitation fields in both historical and RCP45 simulations, for conducting moisture budget analysis.

Figure

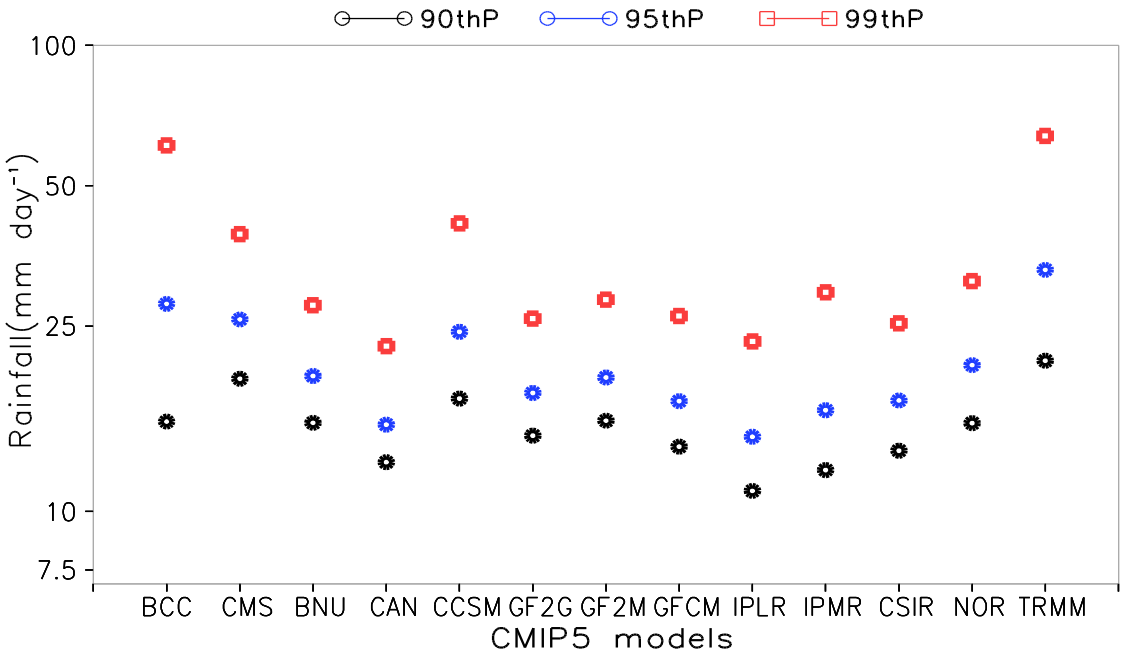

Fig 1: Percentile rainfall intensity for daily time series over the ASM region (60-110°E and 15°S-25°N) from TRMM and historical simulations for selected CMIP5 models. Here BCC stands for BCC-CSM1.1, similarly CMS for CMCC-CMS, BNU for BNU-ESM, CAN for CanESM2, CCSM for CCSM4, GF2G for GFDL-ESM-2G, GF2M for GFDL-ESM-2M, GFCM for GFDL-CM3, IPLR for IPSL-CM5A-LR, IPMR for IPSL-CM5A-MR, CSIR for CSIRO-Mk3.6.0, and finally NOR for NorESM1-M. Note that a log scale is used for the vertical axis and that the unit for this axis is in mm day^{-1}.

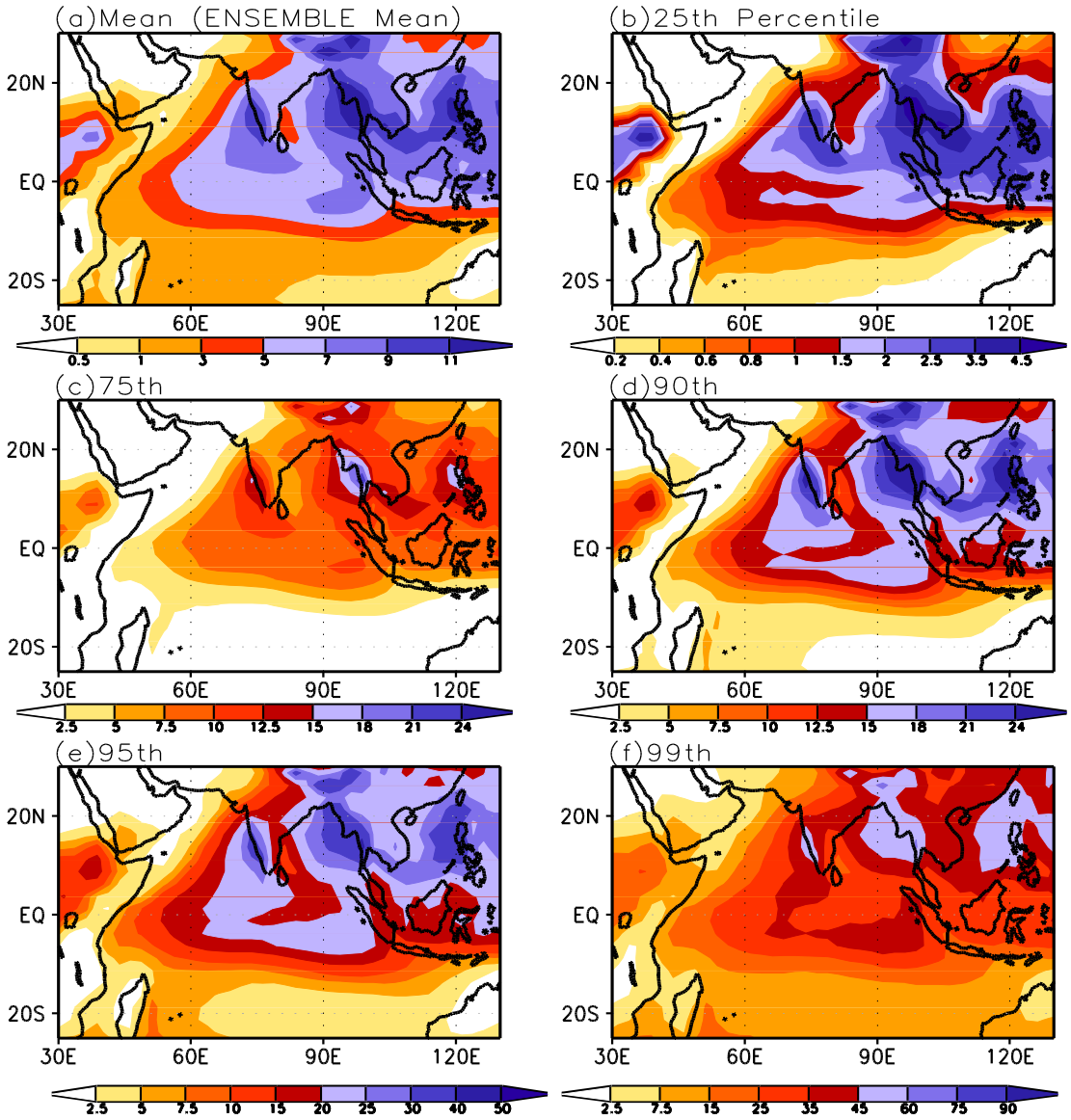

Figure 2: (a) Ensemble mean rainfall (in mm day^{-1}) at seasonal time scale (for JJAS period) for historical simulations using 32 CMIP5 models. (b) to (f) Ensemble mean of rainfall intensities (in mm day^{-1}) at different percentile thresholds using daily rainfall from historical simulations of 32 CMIP5 models, for the JJAS period. See Section 2 for further details about the percentile thresholds definitions.

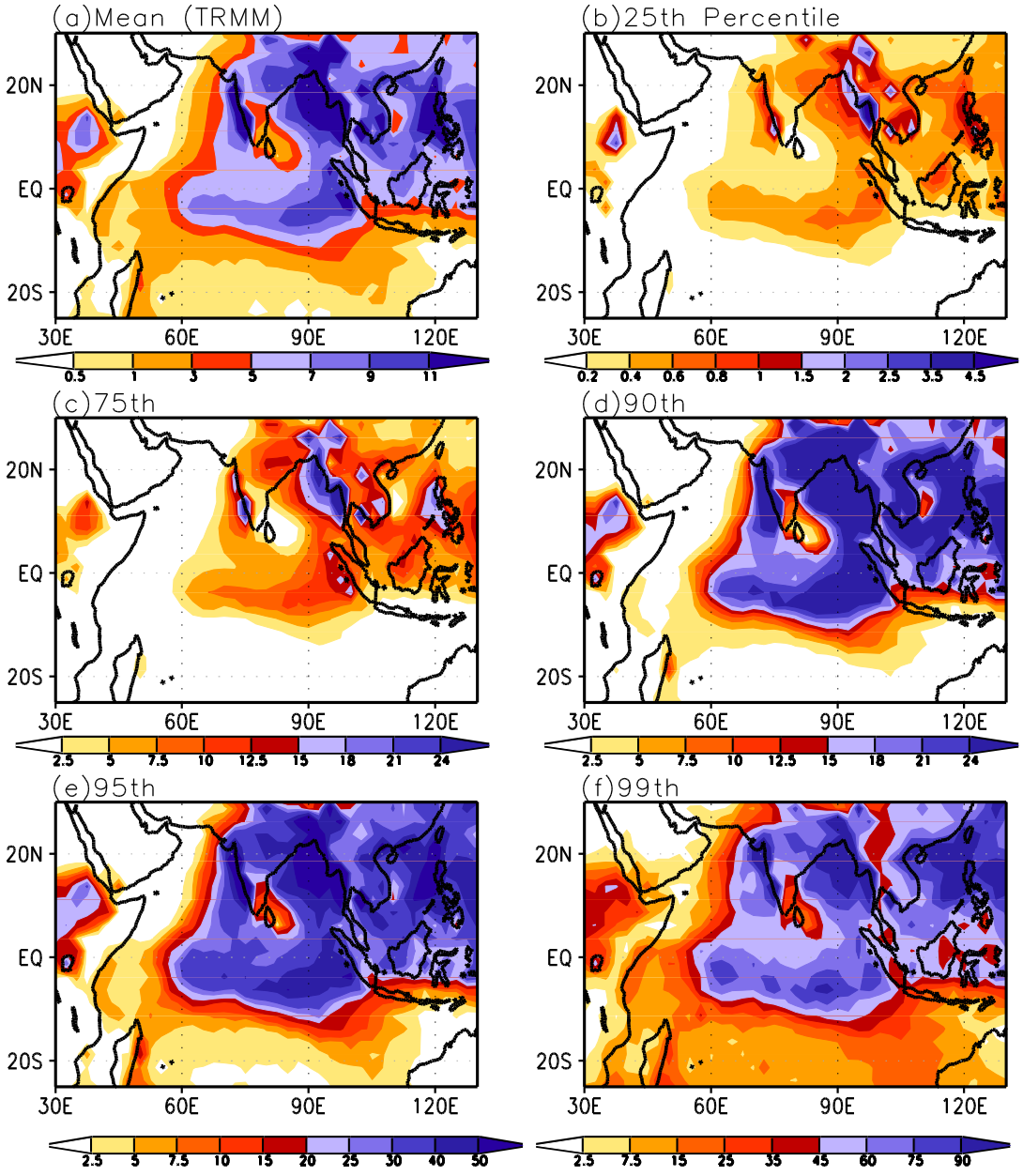

Figure 3: Same as Fig 2, but for TRMM rainfall observations.

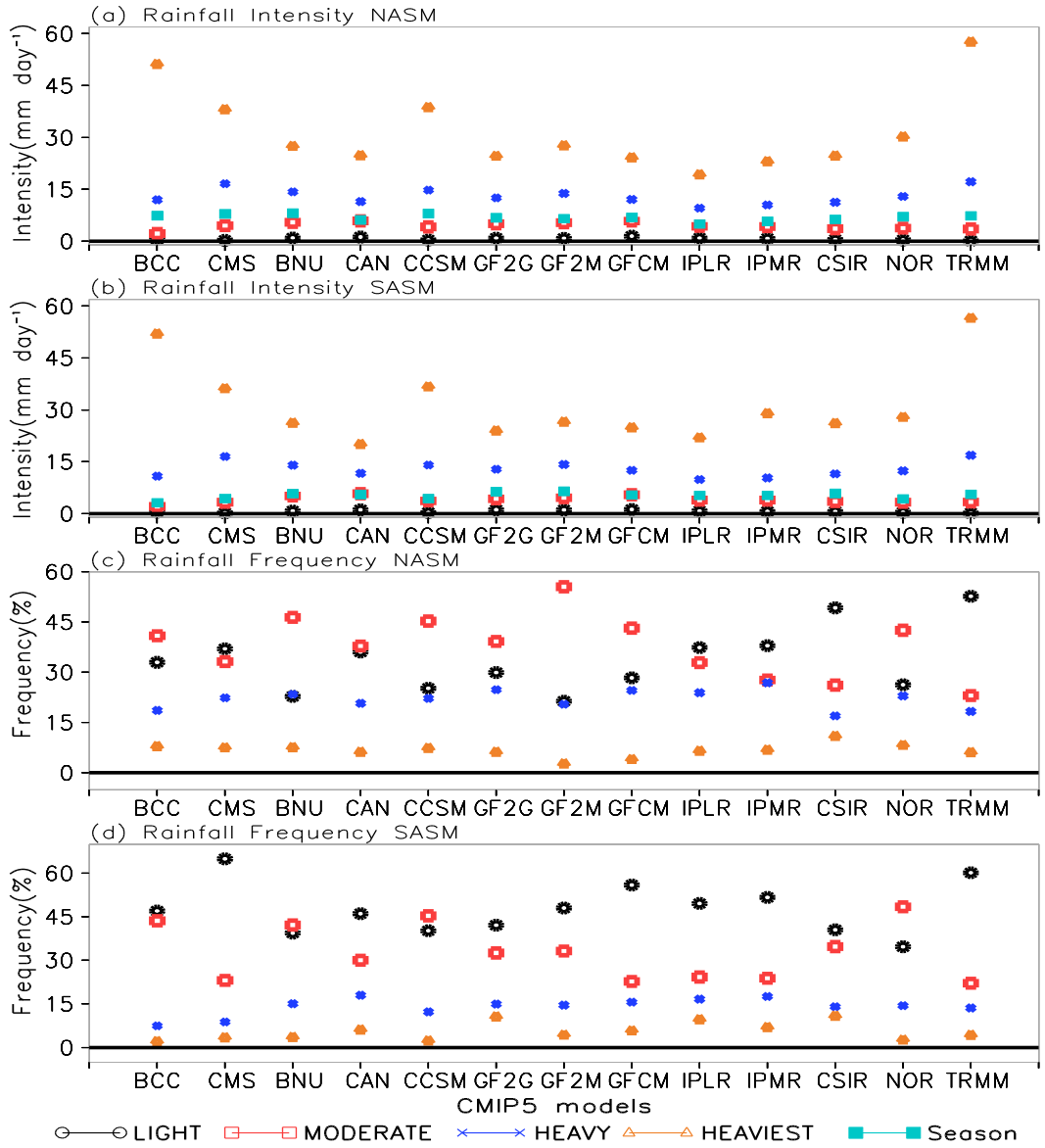

Figure 4a-d: Rainfall intensity of various rainfall events over (a) NASM and (b) SASM domains, for historical simulations using 12 CMIP5 models. (c) and (d) are same as (a) and (b), but for rainfall frequency. Here BCC stands for BCC-CSM1.1, similarly CMS for CMCC-CMS, BNU for BNU-ESM, CAN for CanESM2, CCSM for CCSM4, GF2G for GFDL-ESM-2G, GF2M for GFDL-ESM-2M, GFCM for GFDL-CM3, IPLR for IPSL-CM5A-LR, IPMR for IPSL-CM5A-MR, CSIR for CSIRO-Mk3.6.0, and, finally, NOR for NorESM1-M. The unit for intensity is in mm day^{-1}, while for frequency, it is in percentages.

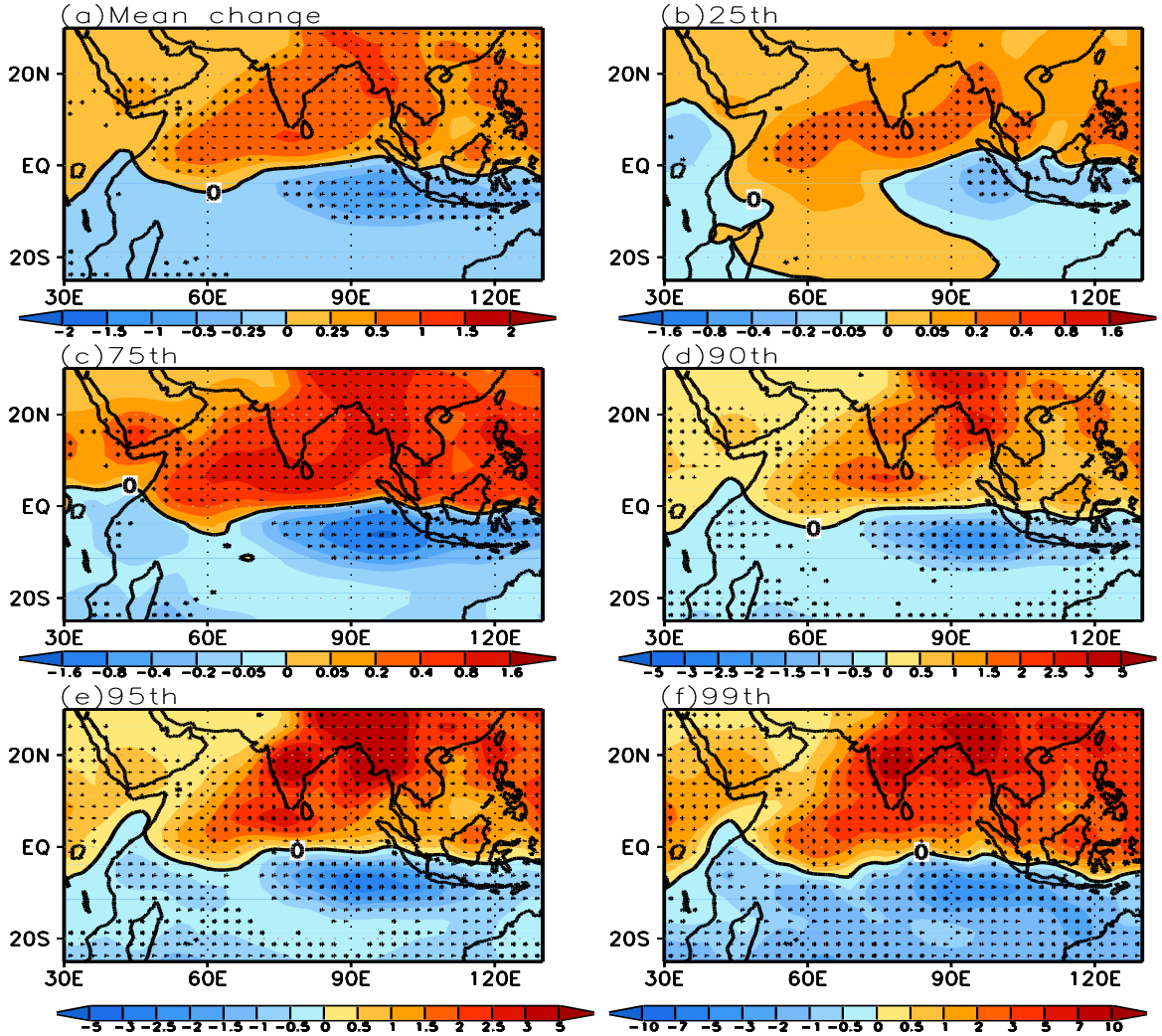

Figure 5: Same as that of Figure 2, but for the future rainfall changes. As explained in the text, the rainfall intensities at various percentile thresholds are derived independently for the historical and RCP4.5 simulations and future change is finally calculated. See the text for more details. Stippling denotes the regions of statistically significant values at the 90% confidence level, using a two tailed student *t*-test for the differences of means using a number of degrees of freedom (DOF) of 62 (e.g. DOF=2×number of models - 2). In other words, each model is assumed to be an independent observation for computing the *t*-statistic. Color shading represents the future changes values**,** without applying any significance test. The thick black contour is the zero isoline.

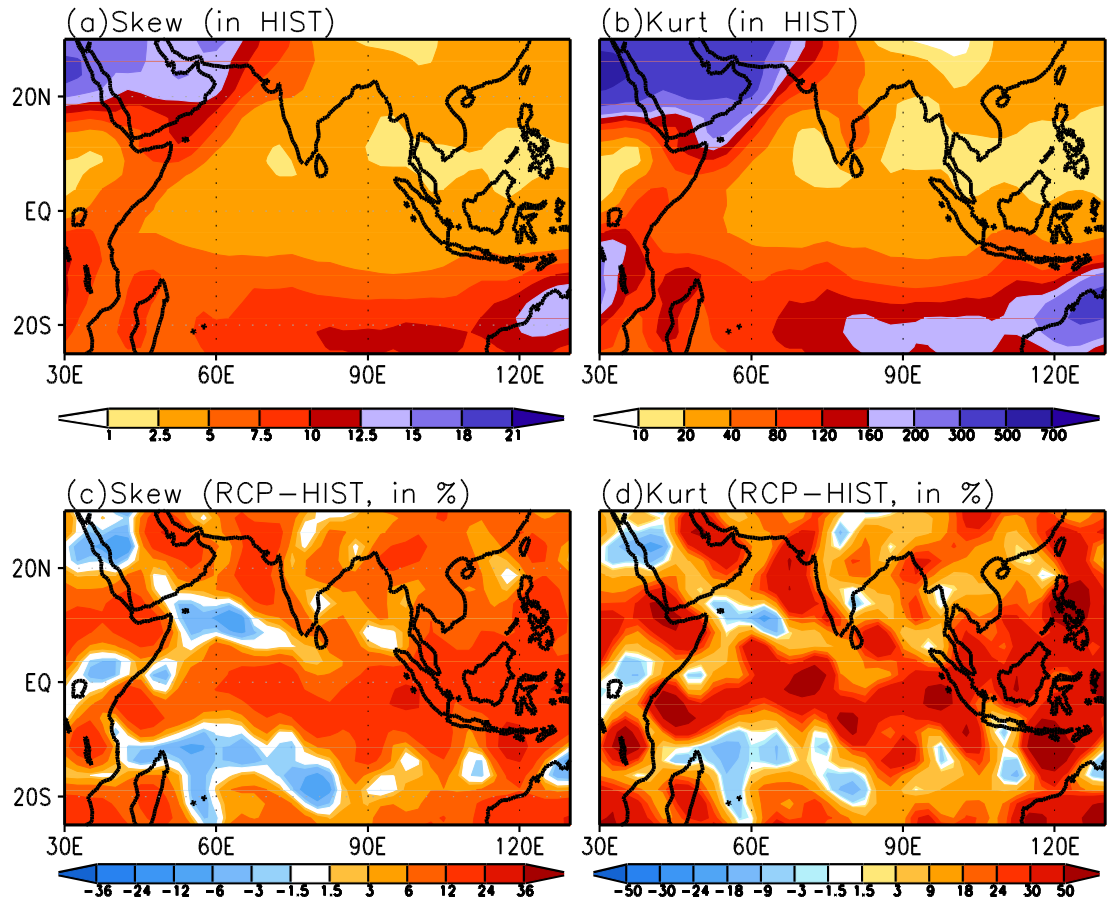

Figure 6: Ensemble mean patterns and their future changes for Kurtosis (a and c) and Skewness (b and d) statistics of rainfall distribution, using 32 CMIP5 models. (a) and (b) for present-day climate. (c) and (d) for future change, expressed in percentages.

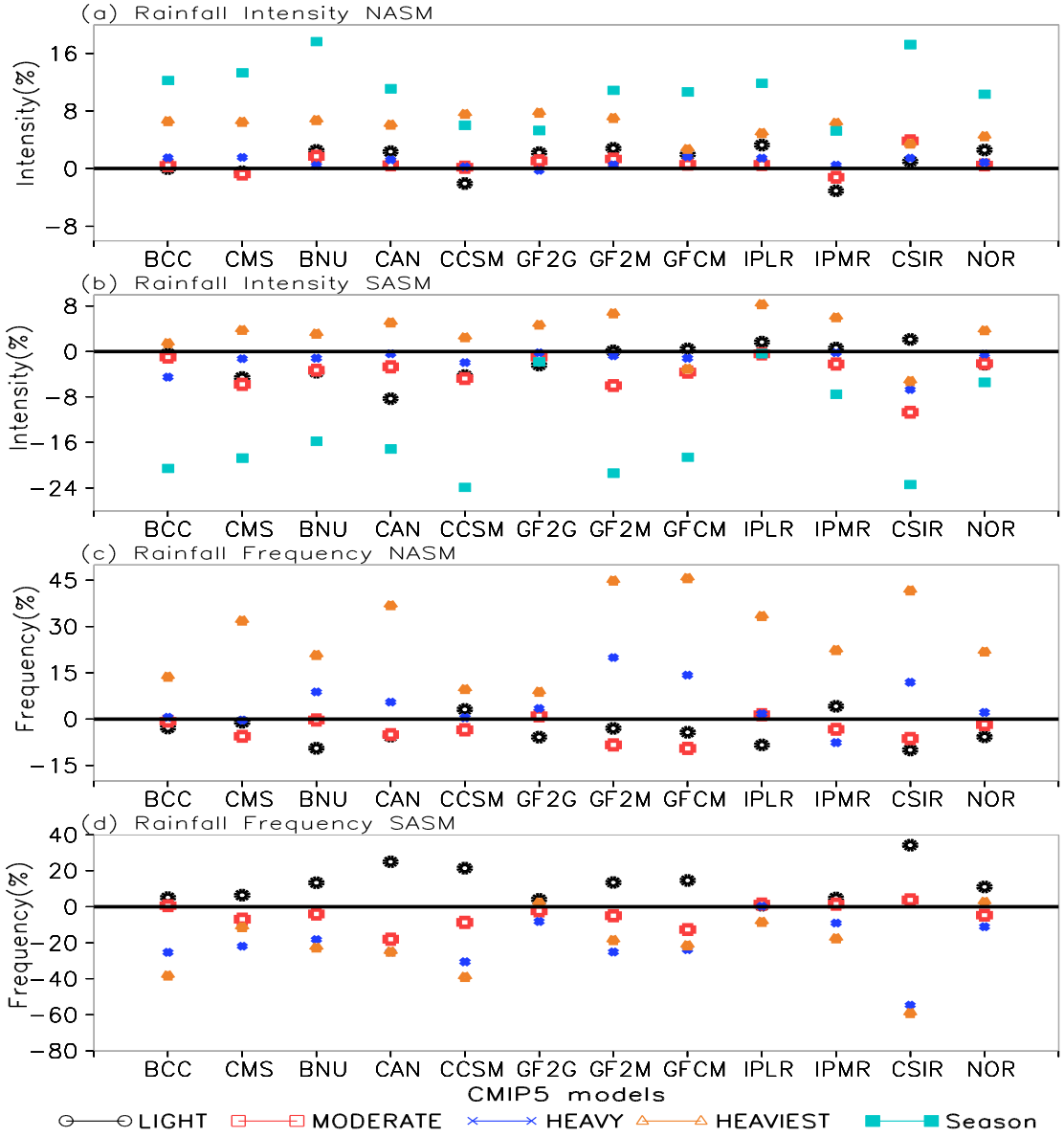

Figure 7a-d: Future change in rainfall intensity (in %) of various rainfall events over (a) NASM and (b) SASM domains. (c) and (d) are same as (a) and (b), but for rainfall frequency (in %). Here BCC stands for BCC-CSM1.1, similarly CMS for CMCC-CMS, BNU for BNU-ESM, CAN for CanESM2, CCSM for CCSM4, GF2G for GFDL-ESM-2G, GF2M for GFDL-ESM-2M, GFCM for GFDL-CM3, IPLR for IPSL-CM5A-LR, IPMR for IPSL-CM5A-MR, CSIR for CSIRO-Mk3.6.0, and, finally, NOR for NorESM1-M.

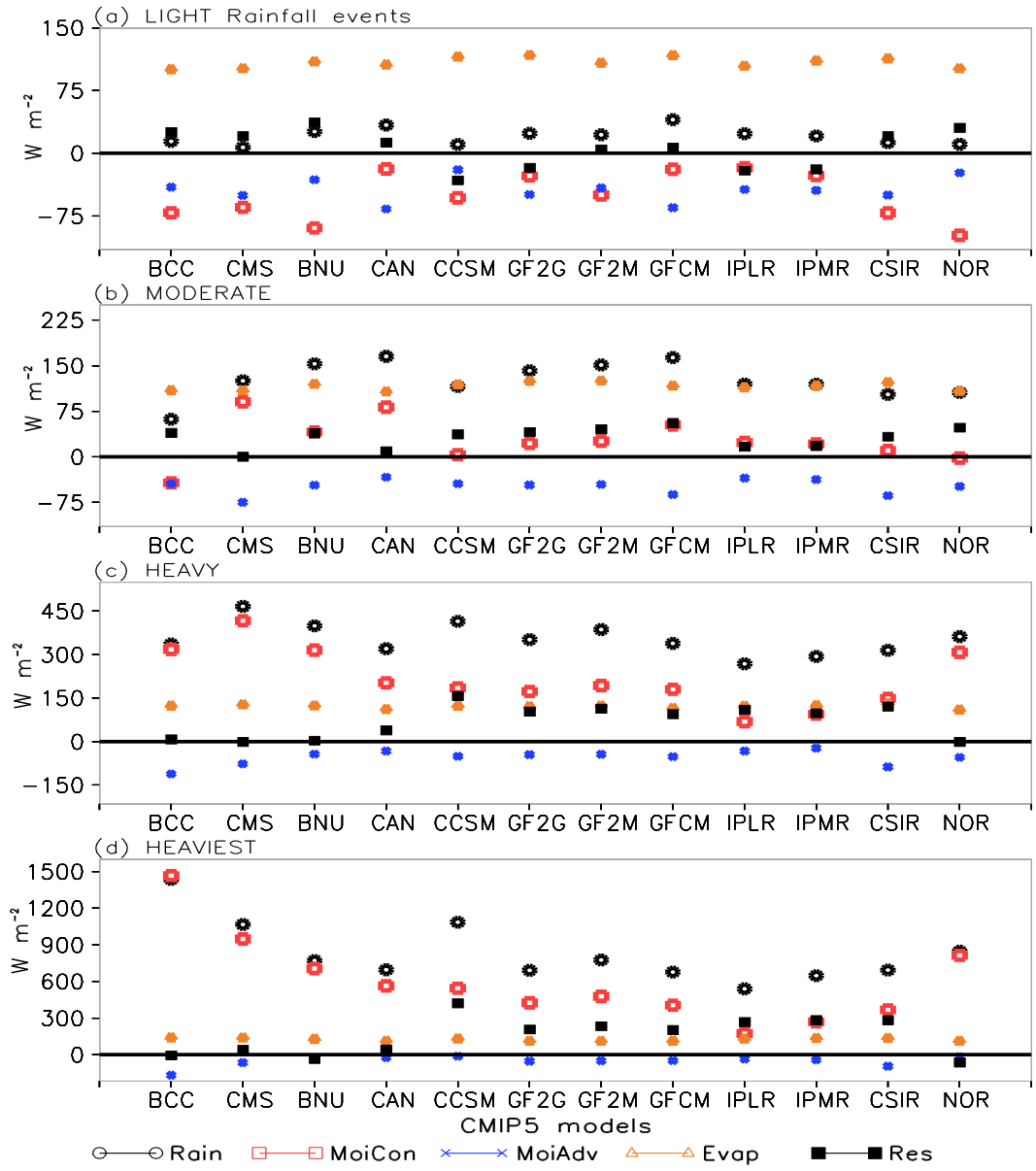

Figure 8a-d: Moisture Budget terms (in W m^{-2}) over NASM region for the present-day climate, as calculated for various rainfall events. MoiCon represents moisture convergence, MoiAdv is for moisture advection, Evap is for evaporation and Res stands for budget residual term. Here BCC stands for BCC-CSM1.1, similarly CMS for CMCC-CMS, BNU for BNU-ESM, CAN for CanESM2, CCSM for CCSM4, GF2G for GFDL-ESM-2G, GF2M for GFDL-ESM-2M, GFCM for GFDL-CM3, IPLR for IPSL-CM5A-LR, IPMR for IPSL-CM5A-MR, CSIR for CSIRO-Mk3.6.0, and, finally, NOR for NorESM1-M.

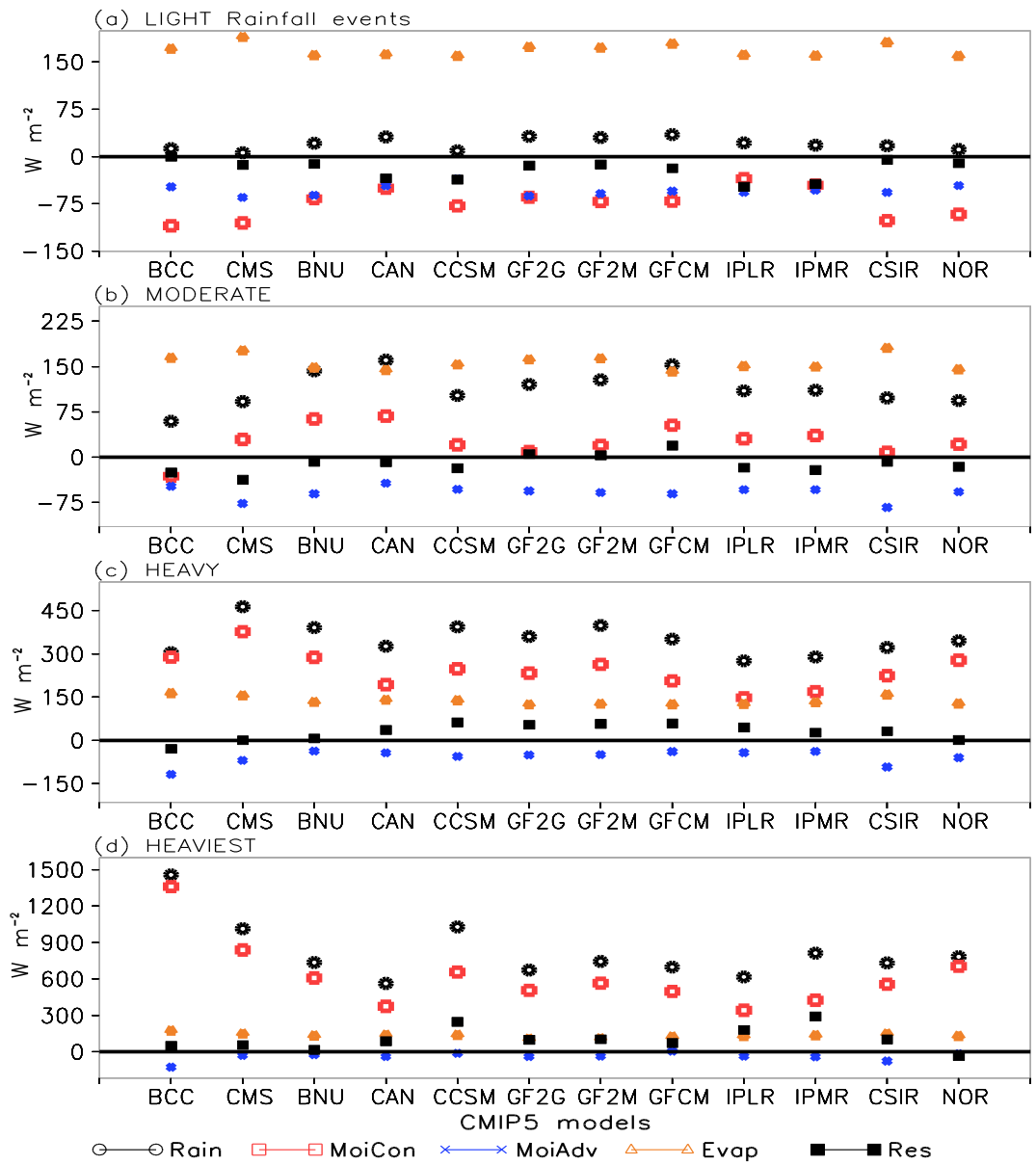

Figure 9a-d: Moisture Budget terms (in W m^{-2}) over SASM region for the present-day climate, as calculated for various rainfall events. MoiCon represents moisture convergence, MoiAdv is for moisture advection, Evap is for evaporation and Res stands for budget residual term. Here BCC stands for BCC-CSM1.1, similarly CMS for CMCC-CMS, BNU for BNU-ESM, CAN for CanESM2, CCSM for CCSM4, GF2G for GFDL-ESM-2G, GF2M for GFDL-ESM-2M, GFCM for GFDL-CM3, IPLR for IPSL-CM5A-LR, IPMR for IPSL-CM5A-MR, CSIR for CSIRO-Mk3.6.0, and, finally, NOR for NorESM1-M.

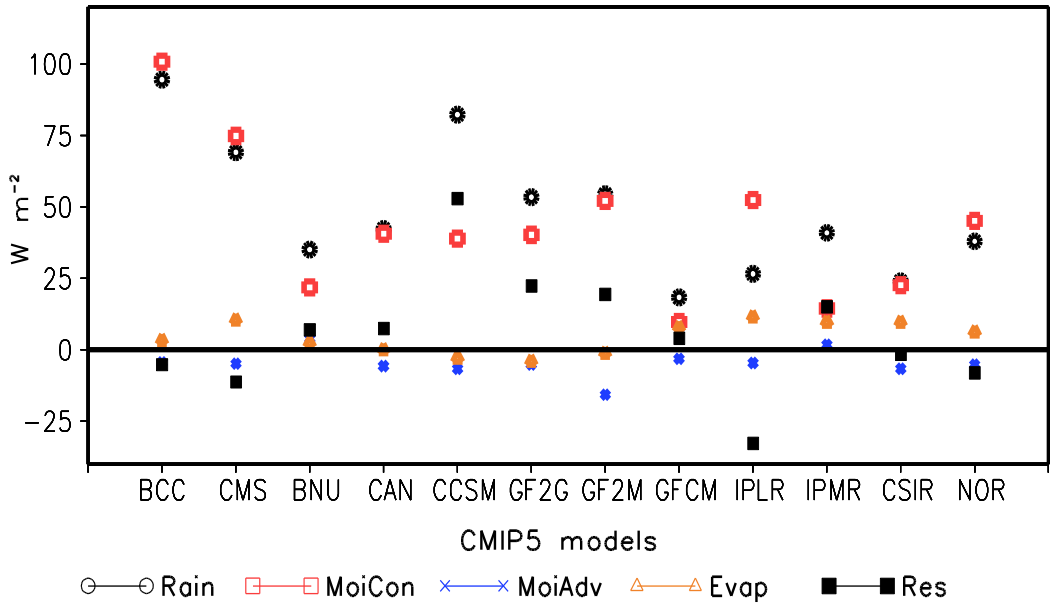

Figure 10: Future changes in moisture Budget terms (in W m^{-2}) over NASM region as calculated for heaviest rainfall intensities. MoiCon represents moisture convergence, MoiAdv is for moisture advection, Evap is for evaporation and Res stands for budget residual term. Here, BCC stands for BCC-CSM1.1, similarly, CMS for CMCC-CMS, BNU for BNU-ESM, CAN for CanESM2, CCSM for CCSM4, GF2G for GFDL-ESM-2G, GF2M for GFDL-ESM-2M, GFCM for GFDL-CM3, IPLR for IPSL-CM5A-LR, IPMR for IPSL-CM5A-MR, CSIR for CSIRO-Mk3.6.0, and, finally, NOR for NorESM1-M.

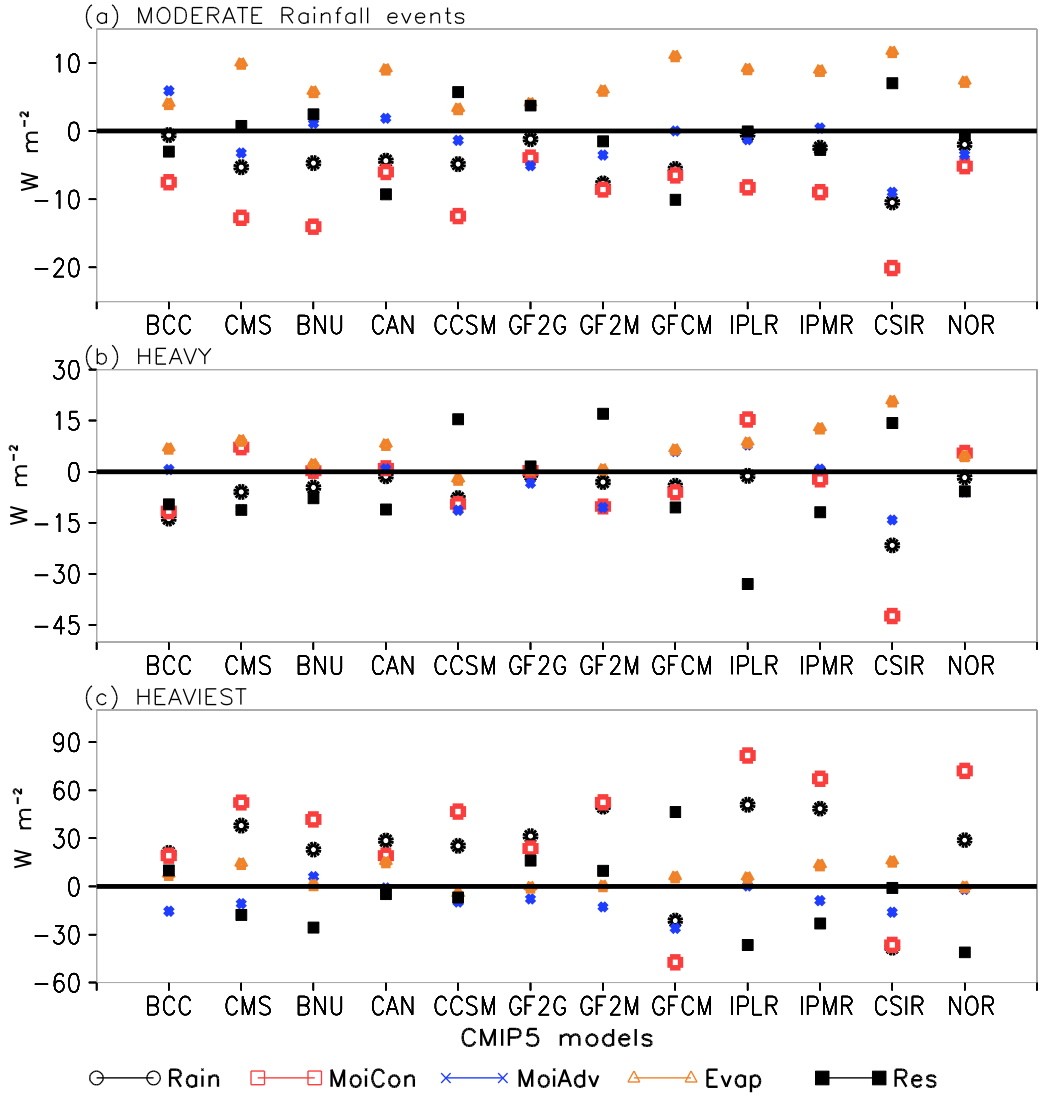

Figure 11a-c: Future changes in moisture Budget terms (in W m^{-2}) over SASM region as calculated for various rainfall events. MoiCon represents moisture convergence, MoiAdv is for moisture advection, Evap is for evaporation and Res stands for budget residual term. Here, BCC stands for BCC-CSM1.1, similarly CMS for CMCC-CMS, BNU for BNU-ESM, CAN for CanESM2, CCSM for CCSM4, GF2G for GFDL-ESM-2G, GF2M for GFDL-ESM-2M, GFCM for GFDL-CM3, IPLR for IPSL-CM5A-LR, IPMR for IPSL-CM5A-MR, CSIR for CSIRO-Mk3.6.0, and, finally, NOR for NorESM1-M.

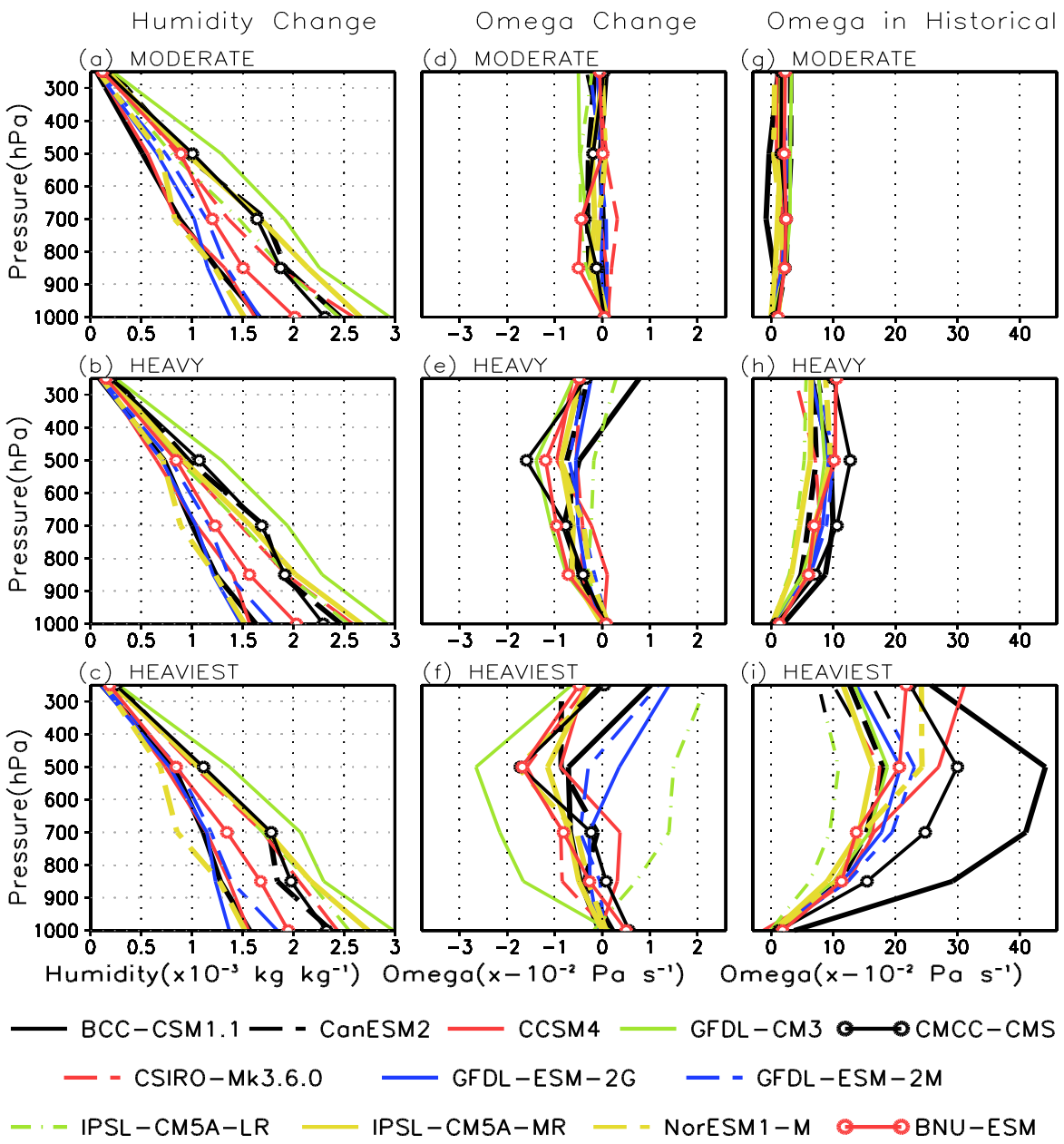

Figure 12a-f: (a)-(f) Vertical profiles of future change in specific humidity (left panels, $\times 10^{-3}$ kg kg^{-1}) and vertical component of velocity (middle panels, $\times$-10^{-2} Pa s^{-1}) over NASM, as calculated for various rainfall events in 12 selected CMIP5 models. (g)-(i) Mean vertical profiles of vertical component of velocity (unit is -10^{-2} Pa s^{-1}) computed from historical simulations of the same 12 CMIP5 models, for various rainfall events over NASM.

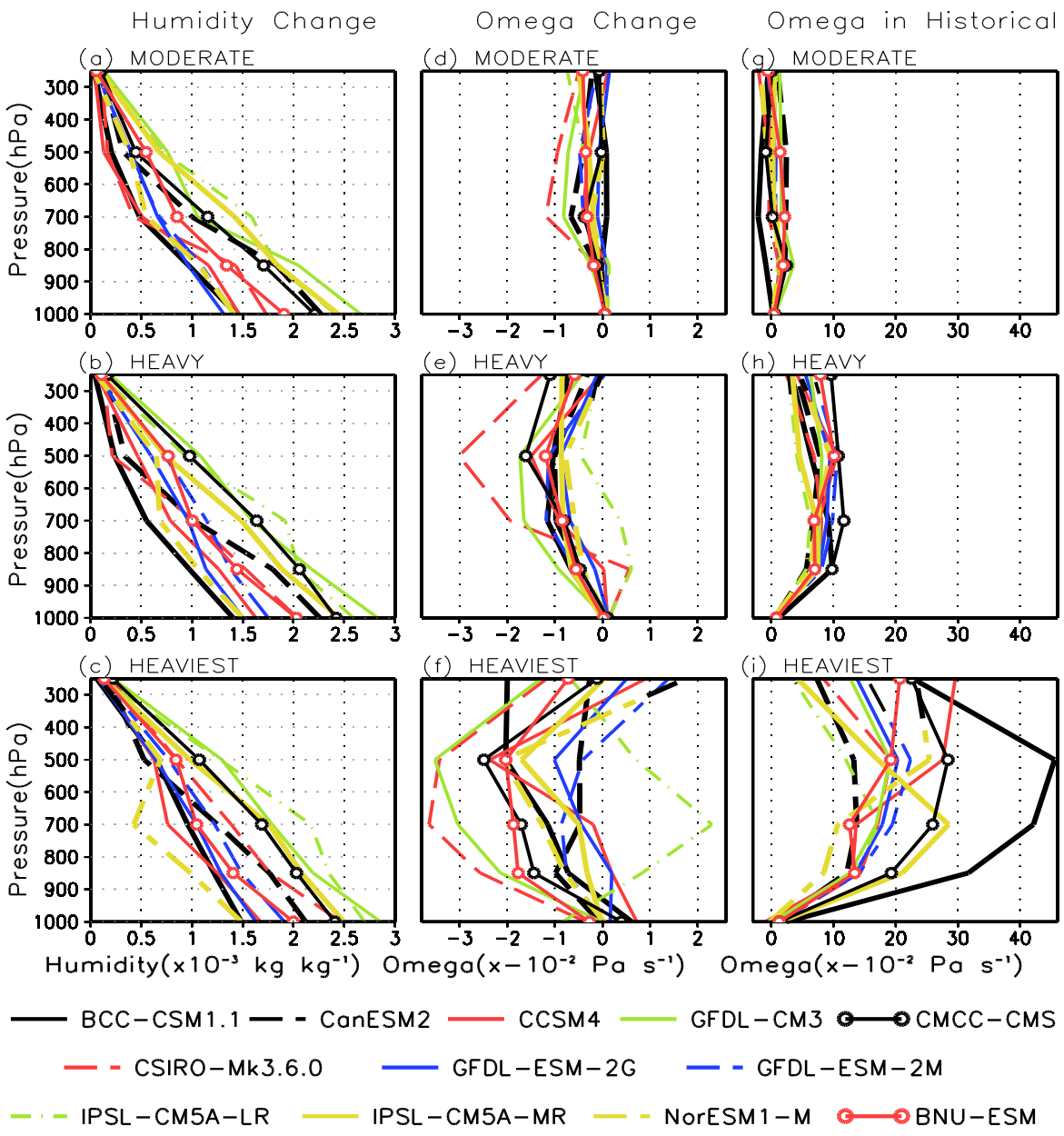

Figure 13a-f: (a)-(f) Vertical profiles of future change in specific humidity (left panels, $\times 10^{-3}$ kg kg^{-1}) and vertical component of velocity (middle panels, $\times$-10^{-2} Pa s^{-1}) over SASM, as calculated for various rainfall events in 12 selected CMIP5 models. (g)-(i) Mean vertical profiles of vertical component of velocity (unit is -10^{-2} Pa s^{-1}) computed from historical simulations of the same 12 CMIP5 models, for various rainfall events over SASM.

Table

No.	Couple model name	Institution	Resolution (Lon×Lat, Levels)
1	ACCESS 1.0	Commonwealth Scientific and Industrial Research Organisation and Bureau of Meteorology Australia	192×145, 38
2	ACCESS 1.3	Commonwealth Scientific and Industrial Research Organisation and Bureau of Meteorology Australia	192×145, 38
3	BCC-CSM1.1	Beijing Climate Center, China Meteorological Administration	128×64, L26
4	BCC-CSM1.1(m)	Beijing Climate Center, China Meteorological Administration	128×64, L26
5	BNU-ESM	Beijing Normal University	T42, L26
6	CanESM2	Canadian Centre for Climate Modelling and Analysis	128×64 , L35
7	CCSM4	National Center for Atmospheric Research	288×192, L26
8	CESM1-BGC	NSF-DOE-NCAR	288 × 192, 27
9	CESM1-CAM5	NSF-DOE-NCAR	288 × 192, 27
10	CMCC-CM	Centro Euro-Mediterraneo sui Cambiamenti Climatici	T159, 31
11	CMCC-CMS	Centro Euro-Mediterraneo sui Cambiamenti Climatici	T63, 95
12	CNRM-CM5	Centre National de Recherches Meteorologiques and Centre Europeen de Recherche et Formation Avancees en Calcul Scientifique	TL127, 31
13	CSIRO-Mk3.6.0	Commonwealth Scientific and Industrial Research Organisation and Queensland Climate Change Centre of Excellence	192×96, L18
14	FGOALS-g2	Institute of Atmospheric Physics- Tsinghua University	128×60, 26
15	GFDL-CM3	Geophysical Fluid Dynamics Laboratory	144×90, L48
16	GFDL-ESM-2G	Geophysical Fluid Dynamics Laboratory	144×90, L24
17	GFDL-ESM-2M	Geophysical Fluid Dynamics Laboratory	144×90, L24
18	GISS-E2-H	NASA Goddard Institute for Space Studies	144×90, 40
19	GISS-E2-R	NASA Goddard Institute for Space Studies	144×90, 40
20	HadGEM2-AO	National Institute of Meteorological Research/ Korea Meteorological Administration	192×145, 60
21	HadGEM2-CC	Met Office Hadley Centre	192×145, 60
22	HadGEM2-ES	Met Office Hadley Centre	192×145, 38
23	INM-CM4	Institute for Numerical Mathematics	180×120, L21
24	IPSL-CM5A-LR	Institut Pierre-Simon Laplace	96×96, 39
25	IPSL-CM5A-MR	Institut Pierre-Simon Laplace	144×143, 39
26	IPSL-CM5B-LR	Institut Pierre-Simon Laplace	96×96, 39
27	MIROC5	Atmosphere and Ocean Research Institute (The University of Tokyo), National Institute for Environmental Studies, and Japan Agency for Marine-Earth Science and Technology	256×128, 40
28	MIROC-ESM	Japan Agency for Marine-Earth Science and Technology, Atmosphere and Ocean Research Institute (The University of Tokyo), and National Institute for Environmental Studies	128×64, 80
29	MIROC-ESM-CHEM	Japan Agency for Marine-Earth Science and Technology, Atmosphere and Ocean Research Institute (The University of Tokyo), and National Institute for Environmental Studies	128×64, 80
30	MPI-ESM-LR	Max Planck Institute for Meteorology (MPI-M)	T63, 47
31	MRI-CGCM3	Meteorological Research Institute	320×160, 48
32	NorESM1-M	Norwegian Climate Centre	144×96, 26

Table 1: Description of the 32 CMIP5 models used in our analysis. The 12 models shown in red are those used for our detailed analysis and those having all the necessary daily atmospheric circulation and precipitation fields in both historical and RCP45 simulations, for conducting moisture budget analysis.